Molecular Column Density Calculation

Jeffrey G. Mangum

National Radio Astronomy Observatory, 520 Edgemont Road, Charlottesville, VA 22903, USA

jmangum@nrao.edu

and

Yancy L. Shirley

Steward Observatory, University of Arizona, 933 North Cherry Avenue, Tucson, AZ 85721, USA

yshirley@as.arizona.edu

May 29, 2013

Received _____; accepted _____

ABSTRACT

We tell you how to calculate molecular column density.

Subject headings: ISM: molecules

Contents

1. Introduction

This document is meant to be a reference for those scientists who need to calculate molecular spectral line column densities. We have organized the document such that some basic background information is first provided to allow a contextural foundation to be lain for further calculations. This foundation includes a basic understanding of radiative transfer and molecular degeneracy, line strength, and hyperfine structure.

2. Radiative and Collisional Excitation of Molecules

When the energy levels of a molecule are in statistical equilibrium, the rate of transitions populating a given energy level is balanced by the rate of transitions which depopulate that energy level. For a molecule with multiple energy levels statistical equilibrium can be written as:

$$n_i \sum_j R_{ij} = \sum_j n_j R_{ji} \tag{1}$$

where n_i and n_j are the populations of the energy levels i and j and R_{ij} and R_{ji} are transition rates between levels i and j. The transition rates contain contributions from:

- Spontaneous radiative excitation (A_{ij})

- Stimulated radiative excitation and de-excitation ($R_{ij} \equiv n_i B_{ij} \int_0^\infty J_\nu \phi_{ij}(\nu) d\nu$)
- Collisional excitation and de-excitation ($n_{collider} C_{ij}$)

where $\phi_\nu(\nu)$ is the line profile function and J_ν is defined as the integral of the specific intensity I_ν over the source of emission:

$$J_\nu \equiv \frac{1}{4\pi} \int I_\nu d\Omega \tag{2}$$

Our statistical equilibrium equation then becomes:

$$n_i \left[\sum_j \left(n_{collider} C_{ij} + B_{ij} \int_0^\infty J_\nu \phi_{ij}(\nu) d\nu \right) + \sum_{j<i} A_{ij} \right] = \sum_j n_j \left(n_{collider} C_{ij} + B_{ji} \int_0^\infty J_\nu \phi_{ji}(\nu) d\nu \right) + \sum_{j>i} n_j A_{ji} \tag{3}$$

For a two-level system with i defined as the lower energy level l and j defined as the upper energy level u, $\sum_{j<i} A_{ij} = 0$ and the statistical equilibrium equation (Equation 3) becomes:

$$n_l \left(n_{collider} C_{lu} + B_{lu} \int_0^\infty J_\nu \phi_{lu}(\nu) d\nu \right) = n_u \left(n_{collider} C_{ul} + B_{ul} \int_0^\infty J_\nu \phi_{ul}(\nu) d\nu + A_{ul} \right) \tag{4}$$

At this point we can derive the Einstein relations A_{ul}, B_{ul}, and B_{lu} by considering only radiative excitation ($C_{lu} = C_{ul} = 0$) and complete redistribution over the line profile ($\phi_{ul}(\nu) = \phi_{lu}(\nu)$). Physically, this means that emitted and absorbed photons are completely independent. Equation 4 then becomes:

$$\begin{aligned} n_l B_{lu} \int_0^\infty J_\nu \phi_{lu}(\nu) &= n_u B_{ul} \int_0^\infty J_\nu \phi_{ul}(\nu) + n_u A_{ul} \\ \int_0^\infty \left[n_l B_{lu} J_\nu \phi_{lu}(\nu) \right] d\nu &= \int_0^\infty \left[n_u B_{ul} J_\nu \phi_{lu}(\nu) + n_u A_{ul} \right] d\nu \\ n_l B_{lu} J_\nu \phi_{lu} &= n_u B_{ul} J_\nu \phi_{lu} + n_u A_{ul} \end{aligned} \tag{5}$$

For a system in thermal equilibrium, the relative level populations follow the Boltzmann distribution:

$$\frac{n_u}{n_l} \equiv \frac{g_u}{g_l} \exp\left(-\frac{h\nu}{kT}\right) \tag{6}$$

and the radiation field J_ν is described by the Planck Function $B_\nu(T)$:

$$B_\nu(T) \equiv \frac{2h\nu^3}{c^2} \left[\exp\left(\frac{h\nu}{kT}\right) - 1 \right]^{-1} \tag{7}$$

Substituting Equations 6 and 7 into Equation 5 (which eliminates the line profile function ϕ_{lu}) yields, after some rearrangement:

$$\left(\frac{c^2}{2h\nu^3} A_{ul} - \frac{g_l}{g_u} B_{lu} \right) \left[\exp\left(\frac{h\nu}{kT}\right) - 1 \right] = \frac{g_l}{g_u} B_{lu} + B_{ul} \tag{8}$$

which implies that:

$$g_l B_{lu} = g_u B_{ul} \tag{9}$$

$$A_{ul} = \frac{2h\nu^3}{c^2} B_{ul} \tag{10}$$

For dipole emission, the spontaneous emission coefficient A_{ul} can be written in terms of the dipole matrix element $|\mu_{lu}|^2$ as:

$$A_{ul} \equiv \frac{64\pi^4\nu^3}{3hc^3}|\mu_{lu}|^2 \tag{11}$$

3. Radiative Transfer

The radiative transfer equation, ignoring scattering processes (such as those involving electrons or dust) is defined as follows (see Spitzer (1978) or Draine (2011) for details):

$$\frac{dI_\nu}{ds} = -\kappa_\nu I_\nu + j_\nu \tag{12}$$

where

$$\begin{aligned}
s &\equiv \text{Path of propagation along the line of sight} \\
I_\nu &\equiv \text{Specific Intensity} \\
\kappa_\nu &\equiv \text{Absorption Coefficient} \\
&= \frac{h\nu}{4\pi}\left(n_l B_{lu} - n_u B_{ul}\right)\phi_\nu &(13)\\
&= \frac{c^2}{8\pi\nu^2}\frac{g_u}{g_l} n_l A_{ul}\left(1 - \frac{g_l n_u}{g_u n_l}\right)\phi_\nu &(14)\\
j_\nu &\equiv \text{Emission Coefficient} \\
&= \frac{h\nu}{4\pi} A_{ul} n_u &(15)
\end{aligned}$$

Since we generally do not know what the propagation path is for our measured radiation it is convenient to change independent variables from pathlength s to "optical depth" τ_ν, which is defined as:

$$d\tau_\nu \equiv \kappa_\nu ds \tag{16}$$

where we use the convention adopted by Draine (2011)[1] that the radiation propagates in the direction of *increasing* optical depth. Switching variables from s to τ_ν in our radiative transfer equation (Equation 12) results in the following radiative transfer equation:

$$dI_\nu = S_\nu d\tau_\nu - I_\nu d\tau_\nu \tag{17}$$

where we define the *Source Function* S_ν:

$$S_\nu \equiv \frac{j_\nu}{\kappa_\nu} \tag{18}$$

By multiplying both sides of Equation 17 by what Draine (2011) has called the "integrating factor" e^{τ_ν}, we can integrate the radiative transfer equation from a starting point where $\tau_\nu = 0$ and $I_\nu = I_\nu(0)$ to find that:

$$\begin{aligned} e^{\tau_\nu}\left(dI_\nu + I_\nu d\tau_\nu\right) &= e^{\tau_\nu} S_\nu d\tau_\nu \\ e^{\tau_\nu} I_\nu - I_\nu(0) &= \int_0^{\tau'} S_\nu d\tau' \\ I_\nu &= I_\nu(0) e^{-\tau_\nu} + \int_0^{\tau'} \exp\left[-\left(\tau_\nu - \tau'\right)\right] S_\nu d\tau' \end{aligned} \tag{19}$$

Equation 19 is a completely general solution to the equation of radiative transfer (again, assuming that scattering is neglected). It defines the intensity measured by the observer (I_ν) as the sum of the background intensity ($I_\nu(0)$) attenuated by the interstellar medium ($\exp\left(-\tau_\nu\right)$) plus the integrated emission ($S_\nu d\tau'$) attenuated by the effective

[1]Draine (2011) points out that Spitzer (1978) uses the opposite convention, that radiation propagates in the direction of *decreasing* optical depth.

absorption due to the interstellar medium between the point of emission and the observer ($\exp\left[-\left(\tau_\nu - \tau'\right)\right]$).

For an infinitely large medium the radiation field would be defined as blackbody: $I_\nu = B_\nu$. If we further assume that the medium through which the radiation is traveling is uniform at an excitation temperature T_{ex}, a condition sometimes referred to as "local thermodynamic equilibrium" (LTE), then the source function S_ν is equivalent to the Planck Function at temperature T_{ex} (Equation 7): $S_\nu = B_\nu(T_{ex})$. Equation 19 becomes:

$$I_\nu = I_\nu(0)e^{-\tau_\nu} + \int_0^{\tau'} \exp\left[-\left(\tau_\nu - \tau'\right)\right] B_\nu(T_{ex}) d\tau' \tag{20}$$

if we further assume that T_{ex} is a constant, Equation 20 becomes:

$$I_\nu = I_\nu(0)\exp(-\tau_\nu) + B_\nu(T_{ex})\left[1 - \exp(-\tau_\nu)\right] \tag{21}$$

In many cases the specific intensity I_ν is replaced by the *Rayleigh-Jeans Equivalent Temperature*, which is the equivalent temperature of a black body at temperature T:

$$J_\nu(T) \equiv \frac{\frac{h\nu}{k}}{\exp\left(\frac{h\nu}{kT}\right) - 1} \tag{22}$$

which results in a form for the radiative transfer equation which involves the observable *Source Radiation Temperature* T_R derived from a differencing measurement:

$$\boxed{J_\nu(T_R) = fJ_\nu(T_{bg})\exp(-\tau_\nu) + fJ_\nu(T_{ex})\left[1 - \exp(-\tau_\nu)\right]} \tag{23}$$

where we have introduced an extra factor f which is the fraction of the spatial resolution of the measurement filled by the source (sometimes called the "filling factor"). See Ulich &

Haas (1976) for a complete derivation of the source radiation temperature for the case of a single antenna position switched measurement.

3.1. The Physical Meaning of Excitation Temperature

The following physical description of the excitation temperature is taken from Harris et al. (2010). The excitation temperature, T_{ex}, is a very general concept that describes an energy density, whether kinetic, radiative, rotational, vibrational, spin, etc.. In observational molecular spectroscopy T_{ex} is the measured quantity; for the rotational transitions of many molecules, the excitation temperature is the rotational temperature T_{rot}. A rigorous definition of "thermalized" emission means that T_{rot} is the same for all transitions of interest. This does not, though, imply that if a transition is thermalized that it is also in thermodynamic equilibrium, with rotational temperature equal to the kinetic temperature of the surrounding H_2 molecules. In a rigorous context, the term subthermal indicates that the excitation temperature T_{rot} for a given transition is below T_{rot} of a comparison transition from the same ensemble of molecules, without reference to T_K, T_{rad}, or any other external energy bath.

4. Column Density

In order to derive physical conditions in the interstellar medium it is often useful to measure the number of molecules per unit area along the line of sight. This quantity, called the "column density", is basically a first-step to deriving basic physical quantities such as spatial density, molecular abundance, and kinetic temperature. Using the two-energy level system defined above, we can express the column density as the number of molecules in energy level u integrated over the pathlength ds:

$$N_u \equiv \int n_u ds \tag{24}$$

Since we want to use our molecular spectral line measurements to calculate the molecular column density, which will ultimately involve the radiative transfer properties of the molecular spectral line measured, we can use the definition of the optical depth (Equation 16), the definition of the absorption coefficient κ (Equation 15), the Boltzmann equation for statistical equilibrium (Equation 6), the definition of the spontaneous emission coefficient A_{ul} (Equation 11), and our definition of the column density (Equation 24) to relate τ_ν to the number of molecules in the upper energy state N_u:

$$\begin{aligned}
\tau_\nu &= \frac{c^2}{8\pi\nu^2}\frac{g_u}{g_l}A_{ul}\phi_\nu \int ds' n_l(s') \left(1 - \frac{g_l n_u(s')}{g_u n_l(s')}\right) \\
&= \frac{c^2}{8\pi\nu^2}\frac{g_u}{g_l}A_{ul}\phi_\nu N_l \left(1 - \frac{g_l N_u}{g_u N_l}\right) \\
&= \frac{c^2}{8\pi\nu^2}\left[\exp\left(\frac{h\nu}{kT}\right) - 1\right] A_{ul}\phi_\nu N_u \\
&= \frac{8\pi^3\nu|\mu_{lu}|^2}{3hc}\left[\exp\left(\frac{h\nu}{kT}\right) - 1\right]\phi_\nu N_u \\
\int \tau_\nu d\nu &= \frac{8\pi^3\nu|\mu_{lu}|^2}{3hc}\left[\exp\left(\frac{h\nu}{kT}\right) - 1\right] N_u
\end{aligned} \tag{25}$$

where in the last step we have integrated over the line profile such that $\int \phi_\nu = 1$. Rearranging and converting our frequency axis to velocity ($\frac{d\nu}{\nu} = \frac{dv}{c}$) in Equation 25, we get an expression for the column density of molecules in the upper transition state (N_u):

$$\boxed{N_u = \frac{3h}{8\pi^3|\mu_{lu}|^2}\left[\exp\left(\frac{h\nu}{kT}\right) - 1\right]^{-1} \int \tau_\nu dv} \tag{26}$$

At this point we have our basic equation for the number of molecules in the upper energy state u of our two-level system. In order to relate this to the total molecular column

density as measured by the intensity of a transition at frequency ν, we need to relate the number of molecules in the upper energy level u (N_u) to the total population of all energy levels in the molecule N_{tot}. Assuming detailed balance at a constant temperature defined by the excitation temperature T_{ex}, we can relate these two quantities as follows:

$$\frac{N_{tot}}{N_u} = \frac{Q_{rot}}{g_u} \exp\left(\frac{E_u}{kT_{ex}}\right) \tag{27}$$

where we have introduced the "rotational partition function" Q_{rot}, a quantity that represents a statistical sum over all rotational energy levels in the molecule (see §6) and g_u, the degeneracy of the energy level u. Substituting for N_u in Equation 27, the total molecular column density becomes:

$$\boxed{N_{tot} = \frac{3h}{8\pi^3|\mu_{lu}|^2} \frac{Q_{rot}}{g_u} \exp\left(\frac{E_u}{kT_{ex}}\right) \left[\exp\left(\frac{h\nu}{kT_{ex}}\right) - 1\right]^{-1} \int \tau_\nu dv} \tag{28}$$

In the following we show how to calculate the level degeneracy g_u (§5), the rotational partition function $Q_{rot} \equiv \sum_i g_i \exp\left(-\frac{E_i}{kT}\right)$ (§6), the dipole matrix element $|\mu_{lu}|^2$ and associated line strength S and dipole moment μ (such that $|\mu_{jk}|^2 \equiv S\mu^2$; §7). Derivation of these terms then allows one to calculate the molecular column density using Equation 28. Following these discussions we derive several commonly-used approximations to Equation 28, including optically thin, optically thick, and the Rayleigh-Jeans approximation. We then close this discussion by working through several examples. We also discuss some minor issues related to the assumed line profile function (Appendix A), the relationship between integrated fluxes and brightness temperatures (Appendix B, and the uncertainty associated with an integrated intensity measurement (Appendix C) in the appendices. In a calculation which utilizes the column density calculation formalism presented below, Appendix D describes the standard three-level model for low-temperature NH_3 excitation often used

to derive the kinetic temperature from measurements of the (1,1) and (2,2) inversion transitions of that molecule.

5. Degeneracies

For rotational molecular transitions the total degeneracy for an an energy level of a transition is given by the product of rotational (g_J and g_K) and spin (g_I) degeneracies:

$$g_u \equiv g_J g_K g_I \tag{29}$$

In the following we derive the expressions for these three contributions to the degeneracy of a molecular energy level.

5.1. Rotational Degeneracy (g_J)

The rotational degeneracy associated with the internal quantum number J, g_J, exists in all molecules and is given by:

$$g_J = 2J_u + 1 \tag{30}$$

5.2. K Degeneracy (g_K)

The K degeneracy (g_K) describes the degeneracy associated with the internal quantum number K in symmetric and asymmetric top molecules. Because of the opposite symmetry of the doubly-degenerate levels for which $K \neq 0$, g_K is defined as follows:

$$\begin{aligned} g_K &= 1 \text{ for K=0 and all linear and asymmetric top molecules} \\ &= 2 \text{ for K}\neq 0 \text{ in symmetric top molecules only} \end{aligned} \tag{31}$$

K-level doubling removes the K degeneracy in asymmetric top molecules.

5.3. Nuclear Spin Degeneracy (g_I)

The nuclear spin degeneracy g_I takes account of the statistical weights associated with identical nuclei in a nonlinear molecule with symmetry (which most nonlinear molecules have). For a molecule with *no symmetry or hyperfine splitting*, each rotational level will have a nuclear spin degeneracy given by:

$$\begin{aligned} g_n &= \prod_i (2I_i + 1) \\ &= (2I+1)^\sigma \end{aligned} \tag{32}$$

$$g_I \equiv \frac{g_{nuclear}}{g_n} \tag{33}$$

where I_i represents the spin of the ith nucleus, σ is the number of identical nuclei, and $g_{nuclear}$ is given in Table 1 for two of the largest classes of molecules found in the interstellar medium medium: those with two (C_{2v} symmetry[2]) and three (C_{3v} symmetry) identical nuclei. Symmetry and hyperfine splitting changes g_n for all practical cases.

[2]The number of symmetry states for a molecule are determined by the number of configurations within which the wavefunction of the molecule is unchanged with a rotation of π about a symmetry axis and a reflection of π through that symmetry plane.

Hyperfine splitting is covered elsewhere in this document, while symmetry considerations are well-covered by Gordy & Cook (1984) (Chapter III.4). See also Turner (1991) for a general discussion applicable to the high-temperature limit.

Keep in mind that if you are only interested in studying one symmetry state (i.e. the para species) of a molecule, $g_I = 1$. In the following we list some examples of $g_{nuclear}$ calculations for several molecules.

5.3.1. H_2CO and C_3H_2

Formaldehyde (H_2CO) is a (slightly) prolate asymmetric top molecule, while Cyclopropenylidene (C_3H_2) is an oblate asymmetric top molecule. Both have two opposing identical H (spin=$\frac{1}{2}$) nuclei. The coordinate wavefunction is symmetric/asymmetric for K_{-1} even/odd, respectively. Therefore, from the two identical spin $\frac{1}{2}$ nuclei cases in Table 1:

$$g_{nuclear} = (2I+1)I = 1 \text{ for } K_{-1} \text{ even} \quad (34)$$

$$= (2I+1)(I+1) = 3 \text{ for } K_{-1} \text{ odd} \quad (35)$$

5.3.2. NH_3 and CH_3CN

Ammonia (NH_3) and Acetonitrile (CH_3CN) are symmetric top molecules with three opposing identical H (spin=$\frac{1}{2}$) nuclei. Therefore, from the three identical spin $\frac{1}{2}$ nuclei cases in Table 1:

Table 1. Nuclear Statistical Weight Factors for C_{2v} and C_{3v} Molecules[a]

Identical Nuclei (σ)[b]	Spin	J	K[c]	$g_{nuclear}$
2	$\frac{1}{2}, \frac{3}{2}, \ldots$	Any	Even	$(2I+1)I$
2	$\frac{1}{2}, \frac{3}{2}, \ldots$	Any	Odd	$(2I+1)(I+1)$
2	$0, 1, 2, \ldots$	Any	Odd	$(2I+1)(I+1)$
2	$0, 1, 2, \ldots$	Any	Even	$(2I+1)I$
3	Any	Even	3n	$\frac{1}{3}(2I+1)(4I^2+4I+3)$
3	Any	Even or Odd	$\neq$ 3n	$\frac{1}{3}(2I+1)(4I^2+4I)$

[a]Derived from Gordy & Cook (1984), Table 3.2 and 3.3.

[b]$g_I \equiv \frac{g_{nuclear}}{(2I+1)^\sigma}$

[c]Where n is an integer.

$$g_{nuclear} = \frac{1}{3}(2I+1)(4I^2+4I+3) = 4 \text{ for K=3n} \quad (36)$$

$$= \frac{1}{3}(2I+1)(4I^2+4I) = 2 \text{ for K}\neq\text{3n} \quad (37)$$

5.3.3. c–C_3H and SO_2

Cyclopropynylidyne (c–C_3H) is an oblate(?) asymmetric top molecule with two opposing identical C (spin=0) nuclei. The coordinate wavefunction is symmetric/asymmetric for K_{-1} even/odd, respectively. Therefore, from the two identical spin 0 nuclei cases in Table 1:

$$g_{nuclear}^{c-C_3H} = (2I+1)I = 0 \text{ for } K_{-1} \text{ even} \quad (38)$$

$$= (2I+1)(I+1) = 1 \text{ for } K_{-1} \text{ odd} \quad (39)$$

This indicates that half of the levels are missing (those for which K_{-1} is even).

6. Rotational Partition Functions (Q_{rot})

For a parcel of gas that exchanges energy with the ambient medium, statistical mechanics states that the partition function Q which describes the relative population of states in the gas is given by:

$$Q = \sum_i g_i \exp\left(-\frac{E_i}{kT}\right) \quad (40)$$

Following Gordy & Cook (1984) (chapter 3, section 3), the partition function for molecules in a gaseous state is a function of the electronic, vibrational, rotational, and

nuclear spin states of the molecule. Assuming that there are no interactions between these states, the total partition function for the molecule can be expressed as the product of the partition functions of these four types of energy states:

$$Q = Q_e Q_v Q_r Q_n \tag{41}$$

Most stable molecules are in ground electronic singlet Σ energy states, making $Q_e = 1$. For simplicity we will also assume that the molecules are in their ground vibrational state ($Q_v = 1$). This leaves us with rotational and nuclear partition functions comprising the total molecular partition function, which we can write as:

$$\begin{aligned} Q_{rot} &\equiv Q_r Q_n \\ &= \sum_{J,K,I} g_J g_K g_I \exp\left(-\frac{E_{JK}}{kT}\right) \end{aligned} \tag{42}$$

where the degeneracies g_J, g_K, and g_I are described in §5.1, §5.2, §5.3, respectively. See Turner (1991) for a nice general discussion listing expressions for Q_{rot} in the high-temperature limit for a variety of molecules.

In the following we derive the rotational partition function Q_{rot} for linear, symmetric, and asymmetric rotor molecules.

6.1. Linear Molecule Rotational Partition Function

For linear molecules:

- $g_J = 2J + 1$ (§5.1)
- $g_K = 1$ (§5.2)

- $g_I = 1$ (since linear molecules with rotational spectra are polar and have no center of symmetry)

which implies that Equation 42 becomes:

$$Q_{rot} = \sum_{J=0}^{\infty} (2J+1) \exp\left(-\frac{E_J}{kT}\right) \tag{43}$$

The energy levels for a linear molecule can be described by a multi-term expansion as a function of $J(J+1)$ (Jennings et al. 1987):

$$E_J = h(B_0 J(J+1) - D_0 J^2(J+1)^2 + H_0 J^3(J+1)^3 - L_0 J^4(J+1)^4 + M_0 J^5(J+1)^5 + ...) \tag{44}$$

where B_0 is the rigid rotor rotation constant and D_0, H_0, L_0, and M_0 are the first- through fourth-order centrifugal distortion constants for the molecule, respectively, all in MHz. Using the rigid rotor approximation to the level energies, thus ignoring all terms other than those linear in J(J+1), Equation 44 becomes:

$$E_J = hB_0 J(J+1) \tag{45}$$

This allows us to approximate Q_{rot} for diatomic linear molecules as follows:

$$\begin{aligned} Q_{rot} &\simeq \sum_{J=0}^{\infty} (2J+1) \exp\left(-\frac{hB_0 J(J+1)}{kT}\right) \\ &\simeq \frac{kT}{hB_0} + \frac{1}{3} + \frac{1}{15}\left(\frac{hB_0}{kT}\right) + \frac{4}{315}\left(\frac{hB_0}{kT}\right)^2 \end{aligned} \tag{46}$$

(from Gordy & Cook (1984) Chapter 3, Equation 3.64). This approximate form is good to 10% for $T > 5\,\mathrm{K}$ (Figure 1).

An alternate approximation for linear polyatomic molecules is derived by McDowell (1988):

$$Q_{rot} \simeq \frac{kT}{hB_0} \exp\left(\frac{hB_0}{3kT}\right) \tag{47}$$

which is reported to be good to 0.01% for $\frac{hB_0}{kT} \lesssim 0.2$ and is good to 1% for $T > 2.8\,\mathrm{K}$ (Figure 1). Note that Equation 47 reduces to Equation 46 when expanded using a Taylor Series.

6.2. Symmetric and Asymmetric Rotor Molecule Rotational Partition Function

For symmetric rotor molecules:

- $g_J = 2J + 1$ (§5.1)
- $g_K = 1$ for K = 0 and 2 for K $\neq$ 0 in symmetric rotors (§5.2)
- $g_K = 1$ for all K in asymmetric rotors
- $g_I = \frac{g_{nuclear}}{(2I+1)^\sigma}$ (See Table 1)

which implies that Equation 42 becomes:

$$Q_{rot} = \sum_{J=0}^{\infty} \sum_{K=-J}^{J} g_K g_I (2J+1) \exp\left(-\frac{E_{JK}}{kT}\right) \tag{48}$$

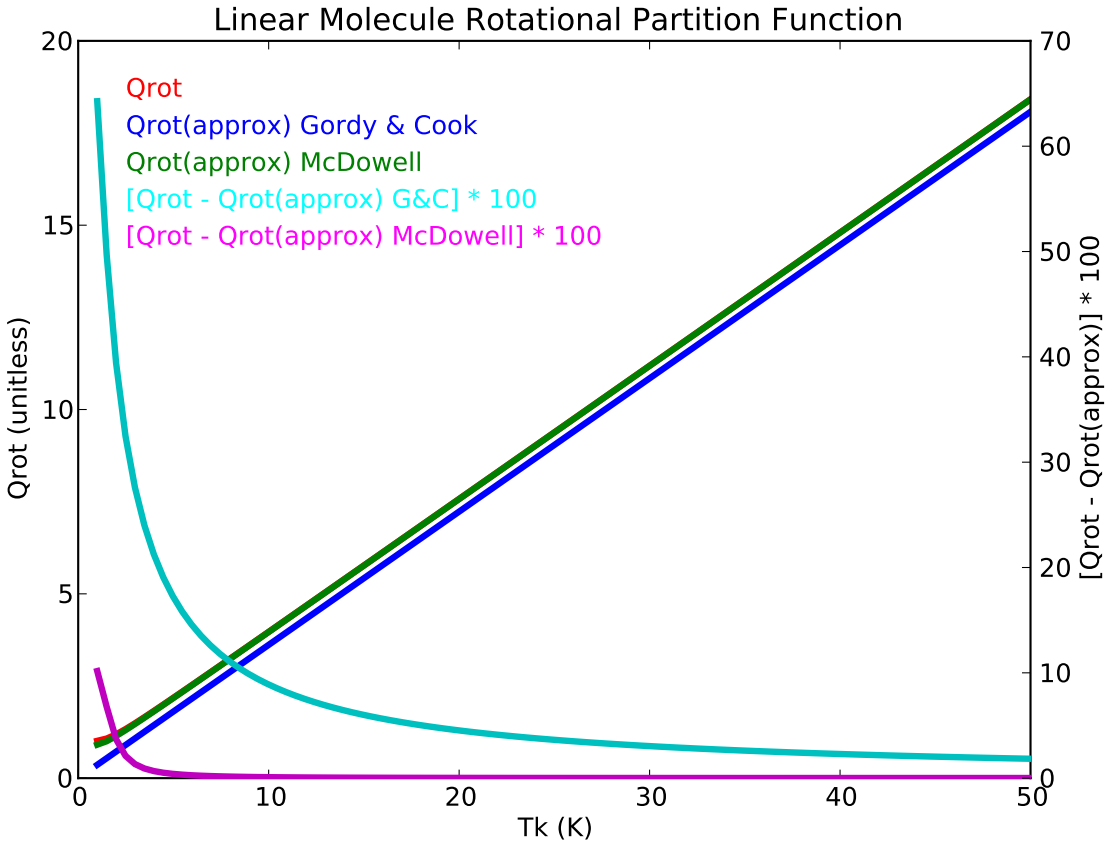

Fig. 1.— Rotational partition function calculations for CO using the lowest 51 levels of the molecule. Shown are Q_{rot} (Equation 43), Q_{rot} given by the expansion of Equation 43 provided by Equation 46, Q_{rot} given by the expansion of Equation 43 provided by Equation 47, and the percentage differences of these to approximations relative to Q_{rot}.

Like the energy levels for a linear molecule, the energy levels for a symmetric rotor molecule can be described by a multi-term expansion as a function of $J(J+1)$:

$$E_{JK} = h(B_0 J(J+1) + s_0 * K^2 + D_j J^2(J+1)^2 + D_{jk} J(J+1)K^2 + D_k K^4 + H_{jkk} J(J+1)K^4 + H_{jjk} J^2(J+1)^2 K^2 + H_{j6} J^3(J+1)^3 + H_{k6} K^6 + ...) \quad (49)$$

where $s_0 \equiv A_0 - B_0$ for a prolate symmetric rotor molecule and $s_0 \equiv C_0 - B_0$ for an oblate symmetric rotor, and the other constants represent various terms in the centrifugal distortion of the molecule. All constants are in MHz. For rigid symmetric rotor molecules, using the rigid rotor approximation to the level energies:

$$E_{JK} = h\left(B_0 J(J+1) + s_0 K^2\right) \quad (50)$$

From McDowell (1990) we can then approximate Q_{rot} for a symmetric rotor molecules as follows:

$$Q_{rot} \simeq \frac{\sqrt{m\pi}}{\sigma} \exp\left(\frac{hB_0(4-m)}{12kT}\right)\left(\frac{kT}{hB_0}\right)^{3/2}\left[1 + \frac{1}{90}\left(\frac{hB_0(1-m)}{kT}\right)^2 + ...\right] \quad (51)$$

where

$$\begin{aligned} m &= \frac{B_0}{A_0} \text{ for a prolate symmetric rotor molecule} \\ &= \frac{B_0}{C_0} \text{ for an oblate symmetric rotor molecule} \\ &= \frac{B_0^2}{A_0 C_0} \text{ for an asymmetric rotor molecule} \end{aligned}$$

If we expand the exponential and take only up to first order terms in the expansion in Equation 51:

$$\begin{aligned} Q_{rot} &\simeq \frac{\sqrt{m\pi}}{\sigma}\left(1+\frac{hB_0(4-m)}{12kT}+...\right)\left(\frac{kT}{hB_0}\right)^{3/2} \\ &\simeq \frac{\sqrt{m\pi}}{\sigma}\left(\frac{kT}{hB_0}\right)^{3/2} \\ &\simeq \frac{1}{\sigma}\left[m\pi\left(\frac{kT}{hB_0}\right)^3\right]^{1/2} \end{aligned} \tag{52}$$

McDowell (1990) notes that this expression is good only for moderate to high kinetic temperatures. This is also the equation for symmetric rotor partition functions quoted by Gordy & Cook (1984) (Chapter 3, Equations 3.68 and 3.69). Figure 2 compares Q_{rot} calculated using Equation 48 and the approximate form given by Equation 52 for NH_3. In this example the approximate form for Q_{rot} (Equation 52) is good to $\lesssim 17\%$ for $T_K > 10\,\mathrm{K}$ and $\lesssim 2.3\%$ for $T_K > 50\,\mathrm{K}$.

7. Dipole Moment Matrix Elements ($|\mu_{jk}|^2$) and Line Strengths (S)

The following discussion is derived from the excellent discussion given in Gordy & Cook (1984), Chapter II.6. A detailed discussion of line strengths for diatomic molecules can be found in Tatum (1986). Spectral transitions are induced by interaction of the electric or magnetic components of the radiation field in space with the electric or magnetic dipole components fixed in the rotating molecule. The strength of this interaction is called the *line strength* S. The matrix elements of the dipole moment with reference to the space-fixed axes (X,Y,Z) for the rotational eigenfunctions ψ_r can be written as follows:

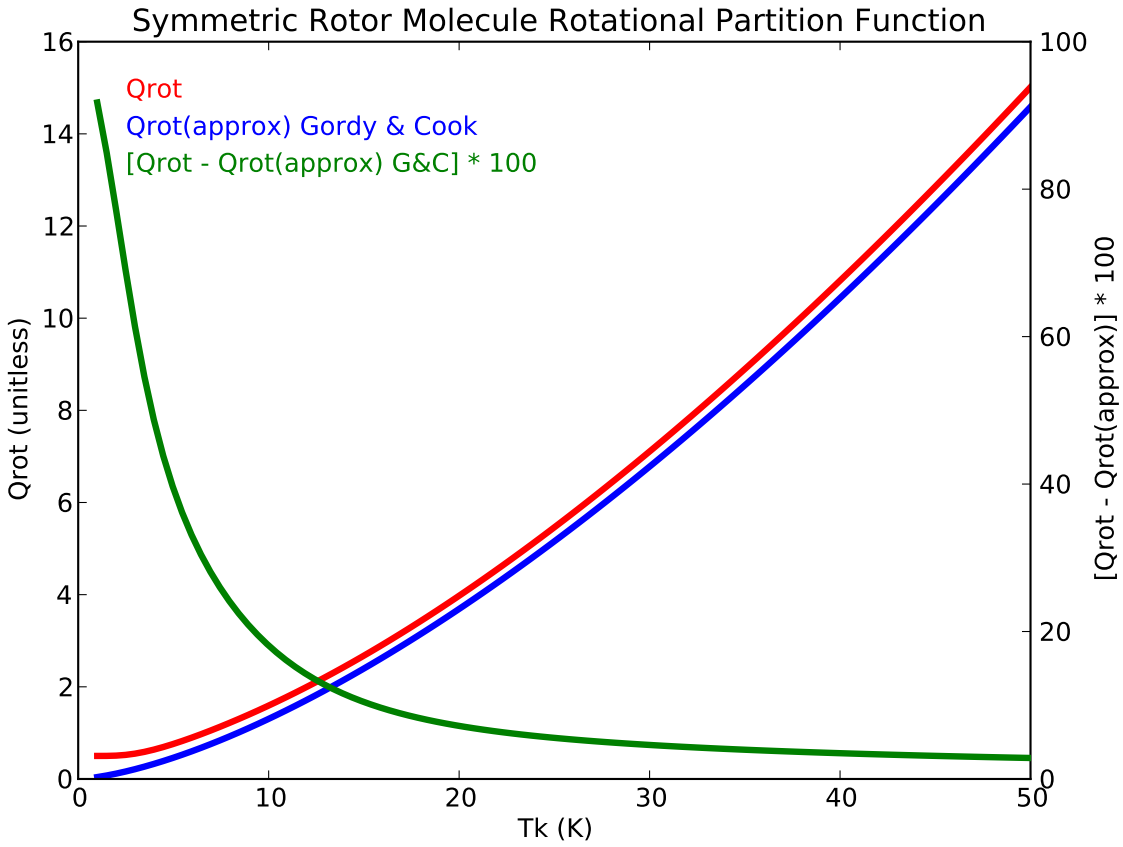

Fig. 2.— Rotational partition function calculations for NH_3 using the lowest 51 levels of the molecule. Shown are Q_{rot} (Equation 48), Q_{rot} given by the Equation 52, and the percentage differences of these to approximations relative to Q_{rot}.

$$\int \psi_r^* \mu_F \psi_r' d\tau = \sum_g \mu_g \int \psi_r^* \Phi_{Fg} \psi_r' d\tau \tag{53}$$

where Φ_{Fg} is the direction cosine between the space-fixed axes F=(X,Y,Z) and the molecule-fixed axes g=(x,y,z). The matrix elements required to calculate line strengths for linear and symmetric top molecules are known and can be evaluated in a straightforward manner, but these calculations are rather tedious because of the complex form of the eigenfunction. Using commutation rules between the angular momentum operators and the direction cosines Φ_{Fg}, Cross et al. (1944) derive the nonvanishing direction cosine matrix elements in the symmetric top representation (J,K,M):

$$\langle J, K, M|\Phi_{Fg}|J', K', M'\rangle = \langle J|\Phi_{Fg}|J'\rangle\langle J, K|\Phi_{Fg}|J', K'\rangle\langle J, M|\Phi_{Fg}|J', M'\rangle \tag{54}$$

The dipole moment matrix element $|\mu_{lu}|^2$ can then be written as:

$$|\mu_{lu}|^2 = \sum_{F=X,Y,Z} \sum_{M'} |\langle J, K, M|\mu_F|J', K', M'\rangle|^2 \tag{55}$$

where the sum over $g = x, y, z$ is contained in the expression for μ_F (Equation 53). Table 2 lists the direction cosine matrix element factors in Equation 54 for symmetric rotor and linear molecules. In the following we give examples of the use of the matrix elements in line strength calculations

8. Linear and Symmetric Rotor Line Strengths

For all linear and most symmetric top molecules, the permanent dipole moment of the molecule lies completely along the axis of symmetry of the molecule ($\mu = \mu_z$). This general

Table 2. Direction Cosine Matrix Element Factors[a] for Linear[b] and Symmetric Top Molecules

Matrix Element Term	J' Value		
	$J+1$	J	$J-1$
$\langle J\|\Phi_{Fg}\|J'\rangle$	$\left\{4(J+1)\left[(2J+1)(2J+3)\right]^{\frac{1}{2}}\right\}^{-1}$	$\left[4J(J+1)\right]^{-1}$	$\left[4J(4J^2+1)\right]^{-1}$
$\langle J,K\|\Phi_{Fz}\|J',K\rangle$	$2\left[(J+1)^2-K^2\right]^{\frac{1}{2}}$	$2K$	$-2(J^2-K^2)^{\frac{1}{2}}$
$\langle J,K\|\Phi_{Fy}\|J',K\pm1\rangle = \mp i\langle J,K\|\Phi_{Fx}\|J',K\pm1\rangle$	$\mp\left[(J\pm K+1)(J\pm K+2)\right]^{\frac{1}{2}}$	$\left[J(J+1)-K(K+1)\right]^{\frac{1}{2}}$	$\mp\left[(J\mp K)(J\mp K-1)\right]^{\frac{1}{2}}$
$\langle J,M\|\Phi_{Zg}\|J',M\rangle$	$2\left[(J+1)^2-M^2\right]^{\frac{1}{2}}$	$2M$	$-2(J^2-M^2)^{\frac{1}{2}}$
$\langle J,M\|\Phi_{Yg}\|J',M\pm1\rangle = \pm i\langle J,M\|\Phi_{Xg}\|J',M\pm1\rangle$	$\mp\left[(J\pm M+1)(J\pm M+2)\right]^{\frac{1}{2}}$	$\left[J(J+1)-M(M+1)\right]^{\frac{1}{2}}$	$\mp\left[(J\mp M)(J\mp M-1)\right]^{\frac{1}{2}}$

[a]Derived from Gordy & Cook (1984), Table 2.1, which is itself derived from Cross et al. (1944).

[b]For linear molecules, set K=0 in the terms listed.

rule is only violated for the extremely-rare "accidentally symmetric top" molecule (where $I_x = I_y$). For all practical cases, then, Equation 55 becomes:

$$|\mu_{lu}|^2 = \mu^2 \sum_{F=X,Y,Z} \sum_{M'} |\langle J, K, M|\Phi_{Fz}|J', K', M'\rangle|^2 \tag{56}$$

8.1. $(\mathbf{J}, \mathbf{K}) \rightarrow (\mathbf{J-1}, \mathbf{K})$ Transitions

Using the matrix element terms listed in the fourth column of Table 2 we can write the terms which make-up Equation 56 for the case $(J, K) \rightarrow (J-1, K)$ as follows:

$$|\mu_{lu}|^2 = \mu^2 \left[\frac{(J^2-K^2)^{1/2}}{J(4J^2-1)^{1/2}}\right] \left\{(J^2-M^2)^{1/2} + \left(\frac{i \pm 1}{2}\right)[(J \mp M)(J \mp M - 1)]^{1/2}\right\} \tag{57}$$

Applying these terms to the dipole moment matrix element (Equation 55, which simply entails squaring each of the three terms in Equation 57 and expanding the $\pm$ terms) and using the definition of $|\mu_{lu}|^2$ (§7):

$$S = \left[\frac{(J^2-K^2)}{J^2(4J^2-1)}\right] \left[(J^2-M^2) + \frac{1}{2}[(J-M)(J-M-1) + (J+M)(J+M-1)]\right] \tag{58}$$

Reducing Equation 58 results in the following for a symmetric top transition $(J, K) \rightarrow (J-1, K)$:

$$\boxed{S = \frac{J^2-K^2}{J(2J+1)} \text{ for } (J, K) \rightarrow (J-1, K)} \tag{59}$$

To derive the equation for a linear molecule transition $J \rightarrow J-1$, simply set $K = 0$ in Equation 59.

8.2. $(\mathbf{J},\mathbf{K}) \rightarrow (\mathbf{J},\mathbf{K})$ Transitions

Using the matrix element terms listed in the third column of Table 2 we can write the terms which make-up Equation 56 for the case $(J,K) \rightarrow (J,K)$ as follows:

$$|\mu_{lu}|^2 = \mu^2 \left[\frac{2K}{4J(J+1)}\right] \left\{(2M) \pm 2\left[J(J+1) - M(M \pm 1)\right]^{1/2}\right\} \tag{60}$$

Applying these terms to the dipole moment matrix element (Equation 55) and using the definition of $|\mu_{lu}|^2$ (§7):

$$S = \left[\frac{K^2}{4J^2(J+1)^2}\right] \left[4M^2 + 2\left[J(J+1) - M(M+1) + J(J+1) - M(M-1)\right]\right] \tag{61}$$

Reducing Equation 61 results in the following for a symmetric top transition $(J,K) \rightarrow (J,K)$:

$$\boxed{S = \frac{K^2}{J(J+1)} \text{ for } (J,K) \rightarrow (J,K)} \tag{62}$$

9. Symmetry Considerations for Asymmetric Rotor Molecules

The symmetry of the total wavefunction ψ for a given rotational transition is determined by the product of the coordinate wavefunction $\psi_e\psi_v\psi_r$ and the nuclear spin wavefunction ψ_n. These wavefunctions are of two types; Fermions and Bosons. Table 3 lists the symmetries for the various wavefunctions in both cases for exchange of two identical nuclei.

Since an asymmetric top can be thought of as belonging to one of two limiting cases, prolate or oblate symmetric, we need to consider these two cases in the context of the coordinate wavefunction $\psi_e\psi_v\psi_r$.

Limiting Prolate: We consider the symmetry of the coordinate wavefunctions with respect to rotation of 180° about the axis of *least* moment of inertia. Since the coordinate wavefunction $\psi_e\psi_v\psi_r$ depends on this rotation angle ξ as $\exp(\pm iK_{-1}\xi)$, it is *symmetric when K_{-1} is even and antisymmetric when K_{-1} is odd.* H_2CO and H_2O are limiting prolate asymmetric top molecules.

Limiting Oblate: We consider the symmetry of the coordinate wavefunctions with respect to rotation of 180° about the axis of *greatest* moment of inertia. Since the coordinate wavefunction $\psi_e\psi_v\psi_r$ depends on this rotation angle ξ as $\exp(\pm iK_{+1}\xi)$, it is *symmetric when K_{+1} is even and antisymmetric when K_{+1} is odd.* NH_2D is a limiting oblate asymmetric top molecule.

10. Hyperfine Structure and Relative Intensities

The relative intensities of the hyperfine transitions of a molecular transition can be calculated using irreducible tensor methods (see Gordy & Cook (1984) Chapter 15). In this section we derive the relative line strengths for the case of $\vec{F} = \vec{J} + \vec{I}$ coupling, where the allowed F energy levels are given by the Clebsch-Gordon Series: $F = J + I, J + I - 1, ..., |J - I|$. The relative intensity is defined such that the sum of the relative intensities of all hyperfine transitions $F' \rightarrow F$ for a given $J' \rightarrow J$ is equal to one:

$$\sum_{F'F} R_i(IJ'F' \rightarrow IJF) = 1. \tag{63}$$

The relative line strengths are calculated in terms of a 6-j symbol,

$$R_i(IJ'F' \rightarrow IJF) = \frac{(2F+1)(2F'+1)}{(2I+1)} \begin{Bmatrix} I & F' & J' \\ I & J & F \end{Bmatrix}^2 . \tag{64}$$

With the aid of the 6-j tables found in Edmonds (1960)[3], and the properties of the 6-j symbols that make them invariant to pair-wise permutation of columns, we find that all single-coupling hyperfine interactions can be described by four 6-j symbols:

Type 1:

$$\begin{Bmatrix} a & b & c \\ 1 & c-1 & b-1 \end{Bmatrix} = (-1)^s \left[\frac{s(s+1)(s-2a-1)(s-2a)}{(2b-1)2b(2b+1)(2c-1)2c(2c+1)} \right]^{\frac{1}{2}}$$

Type 2:

$$\begin{Bmatrix} a & b & c \\ 1 & c-1 & b \end{Bmatrix} = (-1)^s \left[\frac{2(s+1)(s-2a)(s-2b)(s-2c+1)}{2b(2b+1)(2b+2)(2c-1)2c(2c+1)} \right]^{\frac{1}{2}}$$

Type 3:

$$\begin{Bmatrix} a & b & c \\ 1 & c-1 & b+1 \end{Bmatrix} = (-1)^s \left[\frac{(s-2b-1)(s-2b)(s-2c+1)(s-2c+2)}{(2b+1)(2b+2)(2b+3)(2c-1)2c(2c+1)} \right]^{\frac{1}{2}}$$

Type 4:

$$\begin{Bmatrix} a & b & c \\ 1 & c & b \end{Bmatrix} = (-1)^{s+1} \frac{2\left[b(b+1)+c(c+1)-a(a+1)\right]}{\left[2b(2b+1)(2b+2)2c(2c+1)(2c+2)\right]^{\frac{1}{2}}}$$

where $s = a + b + c$. Generalizing this formalism to all single nucleus coupling schemes as follows:

$$Z \mapsto N \quad F \quad F_i \tag{65}$$

$$X \mapsto J \quad F_i \tag{66}$$

$$\vec{Z} = \vec{X} + \vec{I} \tag{67}$$

[3]Many online calculation tools are available that will calculate 6-j symbols. For example, see *http://www.svengato.com/sixj.html*.

we find that the relative intensity of a hyperfine transition is given by

$$R_i = \prod^{HF} \frac{(2Z_u+1)(2Z_l+1)}{(2I+1)} \{6-j\}^2 \tag{68}$$

where the product is taken over all hyperfine interactions which contribute to the transition and i represents each hyperfine transition. Note that R_i has the property that

$$\sum_i R_i = 1 \tag{69}$$

Table 4 shows the correspondence between all $\Delta Z = \pm 1$ and $\Delta X = \pm 1$ transitions and their associated 6-j type listed above. In the following sections we provide illustrative examples of the application of this formalism for calculating relative hyperfine transition intensities.

11. Approximations to the Column Density Equation

In the following we derive several commonly-use approximations to the column density equation 28.

11.1. Rayleigh-Jeans Approximation

Assume that $h\nu \ll kT_{ex}$. This reduces the term in [ ] in Equation 28 to $\frac{h\nu}{kT_{ex}}$, and reduces the radiative transfer equation (Equation 23) to

$$J(T_R) = f\,[J(T_{ex}) - J(T_{bg})]\,[1-\exp(-\tau)] \tag{70}$$

$$T_R = f\,[T_{ex} - T_{bg}]\,[1-\exp(-\tau)] \tag{71}$$

Table 3. Eigenfunction Symmetries for Exchange of Two Identical Nuclei[a]

		Wavefunction[b]			
Statistics	Spin (I)	Total (ψ)	Coordinate ($\psi_e\psi_v\psi_r$)	Spin (ψ_n)	$g_{nuclear}$
Fermi	$\frac{1}{2}, \frac{3}{2}, \ldots$	A	S	A	$(2I+1)I$
Fermi	$\frac{1}{2}, \frac{3}{2}, \ldots$	A	A	S	$(2I+1)(I+1)$
Bose	$0, 1, 2, \ldots$	S	S	S	$(2I+1)(I+1)$
Bose	$0, 1, 2, \ldots$	S	A	A	$(2I+1)I$

[a]From Gordy & Cook (1984), Table 3.2.

[b]Key: A = Asymmetric (para); S = Symmetric (ortho).

Table 4. Hyperfine Transition to 6-j Symbol Correspondence

$Z_u \rightarrow Z_l$	$X_u \rightarrow X_l$	a	b	c	Type
$Z+1 \rightarrow Z$	$X+1 \rightarrow X$	I	X+1	Z+1	1
	$X \rightarrow X$	I	X	Z+1	2
	$X-1 \rightarrow X$	I	Z	X	3
$Z \rightarrow Z$	$X+1 \rightarrow X$	I	Z	X+1	2
	$X \rightarrow X$	I	Z	X	4
	$X-1 \rightarrow X$	I	Z	X	2
$Z-1 \rightarrow Z$	$X+1 \rightarrow X$	I	X	Z	3
	$X \rightarrow X$	I	X	Z	2
	$X-1 \rightarrow X$	I	X	Z	1

Equation 28 then reduces to

$$\begin{aligned} N_{tot} &= \frac{3h}{8\pi^3 S\mu^2 R_i}\frac{Q_{rot}}{g_J g_K g_I}\exp\left(\frac{E_u}{kT_{ex}}\right)\frac{k}{h\nu}\int\left[\frac{T_R}{f\left[1-\exp(-\tau)\right]}+T_{bg}\right]\tau_\nu dv \\ &= \frac{3k}{8\pi^3 \nu S\mu^2 R_i}\frac{Q_{rot}}{g_J g_K g_I}\exp\left(\frac{E_u}{kT_{ex}}\right)\int\left[\frac{T_R}{f\left[1-\exp(-\tau)\right]}+T_{bg}\right]\tau_\nu dv \end{aligned} \quad (72)$$

Assuming that the temperature of the background source (i.e. the cosmic microwave background radiation) is small in comparison to the molecular excitation temperature ($T_{bg} \ll T_{ex}$) in Equation 71, Equation 72 becomes:

$$\begin{aligned} N_{tot} &= \frac{3k}{8\pi^3 \nu S\mu^2 R_i}\frac{Q_{rot}}{g_J g_K g_I}\exp\left(\frac{E_u}{kT_{ex}}\right)\int\frac{\tau_\nu T_R}{f\left[1-\exp(-\tau)\right]}dv \\ &\simeq \frac{1.67\times 10^{14} Q_{rot}}{\nu(GHz)S\mu^2(Debye)R_i g_J g_K g_I}\exp\left(\frac{E_u}{kT_{ex}}\right)\int\frac{\tau_\nu T_R dv(km/s)}{f\left[1-\exp(-\tau)\right]}\ \mathrm{cm}^{-2} \end{aligned} \quad (73)$$

11.2. Optically Thin Approximation

Assume $\tau_\nu \ll 1$. The column density equation (Equation 73) becomes

$$\begin{aligned} N_{tot}^{thin} &= \frac{3h}{8\pi^3 S\mu^2 R_i}\frac{Q_{rot}}{g_J g_K g_I}\exp\left(\frac{E_u}{kT_{ex}}\right)\frac{k}{h\nu}\int\frac{T_R}{f}dv \\ &= \frac{3k}{8\pi^3 \nu S\mu^2 R_i}\frac{Q_{rot}}{g_J g_K g_I}\exp\left(\frac{E_u}{kT_{ex}}\right)\int\frac{T_R}{f}dv \end{aligned} \quad (74)$$

11.3. Optically Thick Approximation

Assume $\tau_\nu \gg 1$. The column density equation (Equation 73) becomes

$$N_{tot}^{thick} = \frac{3h}{8\pi^3 S\mu^2 R_i}\frac{Q_{rot}}{g_J g_K g_I}\exp\left(\frac{E_u}{kT_{ex}}\right)\frac{k}{h\nu}\int\frac{\tau T_R}{f}dv$$

$$= \frac{3k}{8\pi^3 \nu S\mu^2 R_i}\frac{Q_{rot}}{g_J g_K g_I}\exp\left(\frac{E_u}{kT_{ex}}\right)\int\frac{\tau T_R}{f}dv \quad (75)$$

$$= N_{tot}^{thin}\frac{\tau}{1-\exp(-\tau)} \quad (76)$$

12. Molecular Column Density Calculation Examples

In the following we describe in detail some illustrative calculations of the molecular column density.

12.1. $C^{18}O$

To derive the column density for $C^{18}O$ from a measurement of its J=1 − 0 transition we use the general equation for molecular column density (28) with the following properties of the $C^{18}O$ J=1 − 0 transition:

$$
\begin{aligned}
S &= \frac{J_u}{2J_u+1} \\
\mu &= 0.1098 \text{ Debye} \\
B_0 &= 57635.96 \text{ MHz} \\
g_u &= 2J_u+1 \\
g_K &= 1 \text{ (for linear molecules)} \\
g_I &= 1 \text{ (for linear molecules)} \\
Q_{rot} &\simeq \frac{kT}{hB}+\frac{1}{3}(Equation\ 46) \\
&\simeq 0.38\,(T+0.88) \\
E_u &= 5.27 \text{ K} \\
\nu &= 109.782182 \text{ GHz}
\end{aligned}
$$

which leads to:

$$N_{tot}(C^{18}O) = \frac{3h}{8\pi^3\mu^2 J_u R_i}\left(\frac{kT_{ex}}{hB}+\frac{1}{3}\right)\exp\left(\frac{E_u}{kT_{ex}}\right)\left[\exp\left(\frac{h\nu}{kT_{ex}}\right)-1\right]^{-1}\int \tau_\nu dv \qquad (77)$$

Assuming that the emission is optically thin ($\tau_\nu \ll 1$; Equation 74), Equation 77 becomes:

$$N_{tot}(C^{18}O) = 4.79\times10^{13}\,(T_{ex}+0.88)\exp\left(\frac{E_u}{kT_{ex}}\right)T_B\Delta v(km/s)\ \text{cm}^{-2} \qquad (78)$$

If we are using integrated fluxes ($S_\nu\Delta v$) instead of integrated brightness temperatures, we use Equation B3:

$$N_{tot}(C^{18}O) = \frac{3c^2}{16\pi^3\Omega_s S\mu^2\nu^3}\left(\frac{Q_{rot}}{g_u g_K g_I}\right)\exp\left(\frac{E_u}{kT}\right)\int S_\nu \Delta v$$
$$= \frac{4.86\times10^{15}\,(T_{ex}+0.88)}{\theta_{maj}(asec)\theta_{min}(asec)}\exp\left(\frac{E_u}{kT_{ex}}\right)S_\nu(Jy)\Delta v(km/s)\ \mathrm{cm}^{-2} \quad (79)$$

12.2. $C^{17}O$

$C^{17}O$ is a linear molecule with hyperfine structure due to interaction with the electric quadrupole moment of the ^{17}O (I = $\frac{5}{2}$) nucleus. Using the selection rule:

$$F = J+I, J+I-1, J+I-2, ..., |J-I|$$

we find that each J-level is split into the hyperfine levels indicated in Table 5 (for the first five J-levels). Since the selection rules for the single-spin coupling case is, $\Delta F = 0, \pm 1$, and $\Delta J = \pm 1$, there are 3, 9, and 14 allowed hyperfine transitions for the $J = 1 \rightarrow 0$, $J = 2 \rightarrow 1$, and $J = 3 \rightarrow 2$ transitions, respectively. Figure 3 shows the energy level structure for the $J = 1 \rightarrow 0$ and $J = 2 \rightarrow 1$ transitions.

We can calculate the relative hyperfine intensities (R_i) for the $J = 1 \rightarrow 0$ and $J = 2 \rightarrow 1$ transitions using the formalism derived in §10. Using Table 4 we can derive the relevant R_i for the electric quadrupole hyperfine coupling cases ($R_i(F, J), I = \frac{5}{2}$; Table 6). Note that in Table 6 we list the relationship between Z and X and their associated quantum numbers following the assignment mapping equations listed in Equation 67. Figure 4 shows the synthetic spectra for the $C^{17}O$ $J = 1 \rightarrow 0$ and $J = 2 \rightarrow 1$ transitions.

To derive the column density for $C^{17}O$ from a measurement of its J=1 − 0 transition we use the general equation for molecular column density (28) with the following properties of the $C^{17}O$ J=1 − 0 F=$\frac{7}{2} - \frac{5}{2}$ transition:

Table 5. Allowed $C^{17}O$ Hyperfine Energy Levels

J	Number of Energy Levels	Allowed F
0	1	$\frac{5}{2}$
1	3	$\frac{7}{2}, \frac{5}{2}, \frac{3}{2}$
2	5	$\frac{9}{2}, \frac{7}{2}, \frac{5}{2}, \frac{3}{2}, \frac{1}{2}$
3	6	$\frac{11}{2}, \frac{9}{2}, \frac{7}{2}, \frac{5}{2}, \frac{3}{2}, \frac{1}{2}$
4	7	$\frac{13}{2}, \frac{11}{2}, \frac{9}{2}, \frac{7}{2}, \frac{5}{2}, \frac{3}{2}, \frac{1}{2}$

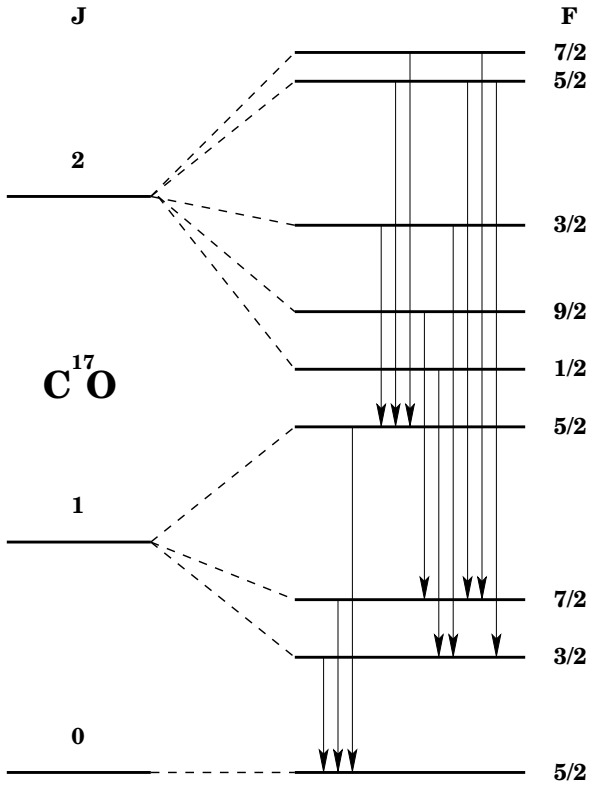

Fig. 3.— Electric quadrupole hyperfine energy level structure for the J=0, 1, and 2 levels of $C^{17}O$. Note that the 3 ($J = 1 \rightarrow 0$) and 9 ($J = 2 \rightarrow 1$) allowed transitions are marked with arrows ordered by increasing frequency from left to right.

Table 6. Hyperfine Intensities[a] for $C^{17}O$ J=1 → 0 and J=2 → 1

$F' \rightarrow F$[b]	$J' \rightarrow J$[b]	a	b	c	Type	$\frac{(2F'+1)(2F+1)}{(2I+1)}$	$\Delta\nu$[c] (kHz)	6j	$R_i(F,J)$
$(\frac{3}{2},\frac{5}{2})$	(1,0)	$\frac{5}{2}$	0	$\frac{5}{2}$	3	4	−501	$-\frac{1}{3\sqrt{2}}$	$\frac{2}{9}$
$(\frac{7}{2},\frac{5}{2})$	(1,0)	$\frac{5}{2}$	1	$\frac{7}{2}$	1	8	−293	$-\frac{1}{3\sqrt{2}}$	$\frac{4}{9}$
$(\frac{5}{2},\frac{5}{2})$	(1,0)	$\frac{5}{2}$	$\frac{5}{2}$	1	2	6	+724	$\frac{1}{3\sqrt{2}}$	$\frac{3}{9}$
$(\frac{3}{2},\frac{5}{2})$	(2,1)	$\frac{5}{2}$	1	$\frac{5}{2}$	3	4	−867	$\frac{1}{10}$	$\frac{1}{25}$
$(\frac{5}{2},\frac{5}{2})$	(2,1)	$\frac{5}{2}$	$\frac{5}{2}$	2	2	6	−323	$-\frac{4\sqrt{2}}{15\sqrt{7}}$	$\frac{64}{525}$
$(\frac{7}{2},\frac{5}{2})$	(2,1)	$\frac{5}{2}$	2	$\frac{7}{2}$	1	8	−213	$\frac{\sqrt{3}}{2\sqrt{35}}$	$\frac{6}{35}$
$(\frac{9}{2},\frac{7}{2})$	(2,1)	$\frac{5}{2}$	2	$\frac{9}{2}$	1	$\frac{40}{3}$	−169	$-\frac{1}{2\sqrt{10}}$	$\frac{1}{3}$
$(\frac{1}{2},\frac{3}{2})$	(2,1)	$\frac{5}{2}$	1	$\frac{3}{2}$	3	$\frac{4}{3}$	−154	$-\frac{1}{2\sqrt{5}}$	$\frac{1}{15}$
$(\frac{3}{2},\frac{3}{2})$	(2,1)	$\frac{5}{2}$	$\frac{3}{2}$	2	2	$\frac{8}{3}$	+358	$\frac{\sqrt{7}}{10\sqrt{2}}$	$\frac{7}{75}$
$(\frac{5}{2},\frac{7}{2})$	(2,1)	$\frac{5}{2}$	1	$\frac{7}{2}$	3	8	+694	$-\frac{1}{6\sqrt{14}}$	$\frac{1}{63}$
$(\frac{7}{2},\frac{7}{2})$	(2,1)	$\frac{5}{2}$	$\frac{7}{2}$	2	2	$\frac{32}{3}$	+804	$\frac{1}{4\sqrt{7}}$	$\frac{2}{21}$
$(\frac{5}{2},\frac{3}{2})$	(2,1)	$\frac{5}{2}$	2	$\frac{5}{2}$	1	4	+902	$-\frac{\sqrt{7}}{15\sqrt{2}}$	$\frac{14}{225}$

[a]The sum of the relative intensities $\sum_i R_i = 1.0$ for each $\Delta J = 1$ transition.

[b]$Z = F$ and $X = J$.

[c]Frequency offsets in kHz relative to 112359.275 and 224714.368 MHz for $J = 1 \rightarrow 0$ and $J = 2 \rightarrow 1$, respectively (from somewhere).

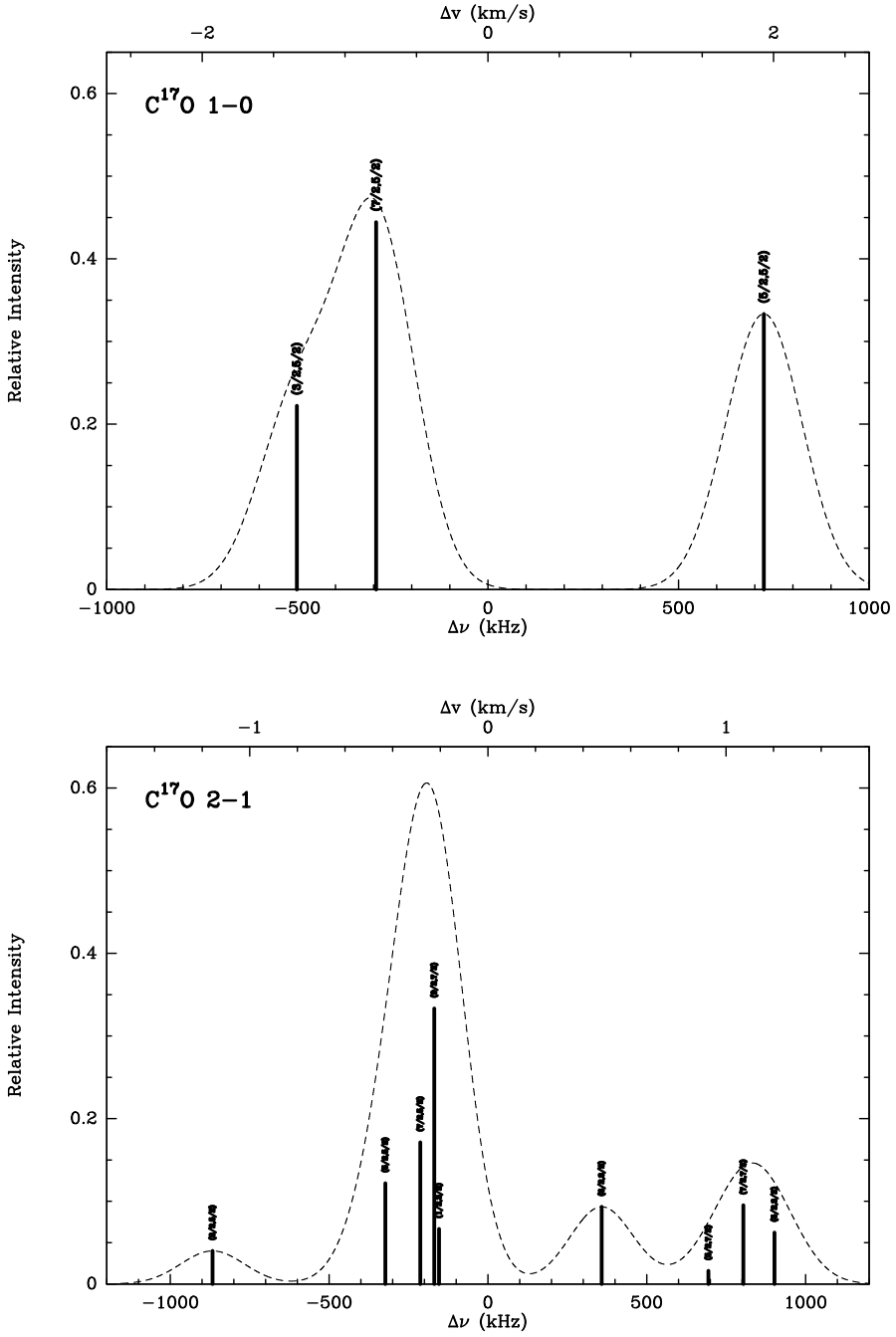

Fig. 4.— Synthetic spectra for the $C^{17}O$ $J = 1 \rightarrow 0$ (top) and $2 \rightarrow 1$ (bottom) transitions. Horizontal axes are offset velocity (top) and frequency (bottom) relative to 112359275.0 and 224714368.0 kHz, respectively. Transition designations in (F′,F) format are indicated. Overlain in dash is a synthetic 100 kHz gaussian linewidth source spectrum.

$$\begin{aligned} S &= \frac{J_u}{2J_u+1} \\ \mu &= 0.11032 \text{ Debye} \\ B_0 &= 56179.99 \text{ MHz} \\ g_J &= 2J_u+1 \\ g_K &= 1 \text{ (for linear molecules)} \\ g_I &= 1 \text{ (for linear molecules)} \\ Q_{rot} &\simeq \frac{kT}{hB}+\frac{1}{3} \text{ (Equation 46)} \\ &\simeq 0.37\,(T+0.90) \\ E_u &= 5.40 \text{ K} \end{aligned} \tag{80}$$

which leads to:

$$N_{tot}(C^{17}O) = \frac{3h}{8\pi^3\mu^2 J_u R_i}\left(\frac{kT_{ex}}{hB}+\frac{1}{3}\right)\exp\left(\frac{E_u}{kT_{ex}}\right)\left[\exp\left(\frac{h\nu}{kT_{ex}}\right)-1\right]^{-1}\int \tau_\nu dv \tag{81}$$

Assuming that the emission is optically thin ($\tau_\nu \ll 1$; Equation 74), Equation 81 becomes:

$$N_{tot}(C^{17}O) = \frac{5.07\times10^{15}\,(T_{ex}+0.88)}{\nu(GHz)R_i}\exp\left(\frac{E_u}{kT_{ex}}\right)T_B\Delta v(km/s)\text{ cm}^{-2} \tag{82}$$

where ν is the frequency of the hyperfine transition used. For example, if the F=$\frac{7}{2}-\frac{5}{2}$ hyperfine was chosen for this calcuation, $R_i = \frac{4}{9}$ (See Table 6) and $\nu = 112359.275 - 0.293$ MHz $= 112.358982$ GHz. Equation 82 then becomes:

$$N_{tot}(C^{17}O) = 1.02\times10^{14}\,(T_{ex}+0.88)\exp\left(\frac{E_u}{kT_{ex}}\right)T_B\Delta v(km/s)\text{ cm}^{-2} \tag{83}$$

12.3. N_2H^+

N_2H^+ is a multiple spin coupling molecule due to the interaction between its spin and the quadrupole moments of the two nitrogen nuclei. For a nice detailed description of the hyperfine levels of the $J = 1 \rightarrow 0$ transition see Shirley et al. (2005). Since the outer N nucleus has a much larger coupling strength than the inner N nucleus, the hyperfine structure can be determined by a sequential application of the spin coupling:

$$\begin{aligned} \vec{F_1} &= \vec{J} + \vec{I_N} \\ \vec{F} &= \vec{F_1} + \vec{I_N} \end{aligned}$$

When the coupling from both N nuclei is considered:

- The $J = 0$ level is split into 3 energy levels,
- The $J = 1$ level is split into 7 energy levels,
- The $J = 2$ and higher levels are split into 9 energy levels.

Since the selection rules for the single-spin coupling case apply, $\Delta F_1 = 0, \pm 1$, $\Delta F = 0, \pm 1$, and $\Delta J = \pm 1$, there are 15, ??, and ?? for the $J = 1 \rightarrow 0$, $J = 2 \rightarrow 1$, and $J = 3 \rightarrow 2$ transitions, respectively. Figure 5 shows the energy level structure for the $J = 1 \rightarrow 0$ transition.

To illustrate the hyperfine intensity calculation for N_2H^+, we derive the relative intensities for the $J = 1 \rightarrow 0$ transition. Relative intensities, derived from Equations 67, 68, and Table 4, are listed in Tables 7, 8, and 9. Figure 6 shows the synthetic spectrum for the N_2H^+ $J = 1 \rightarrow 0$ transition.

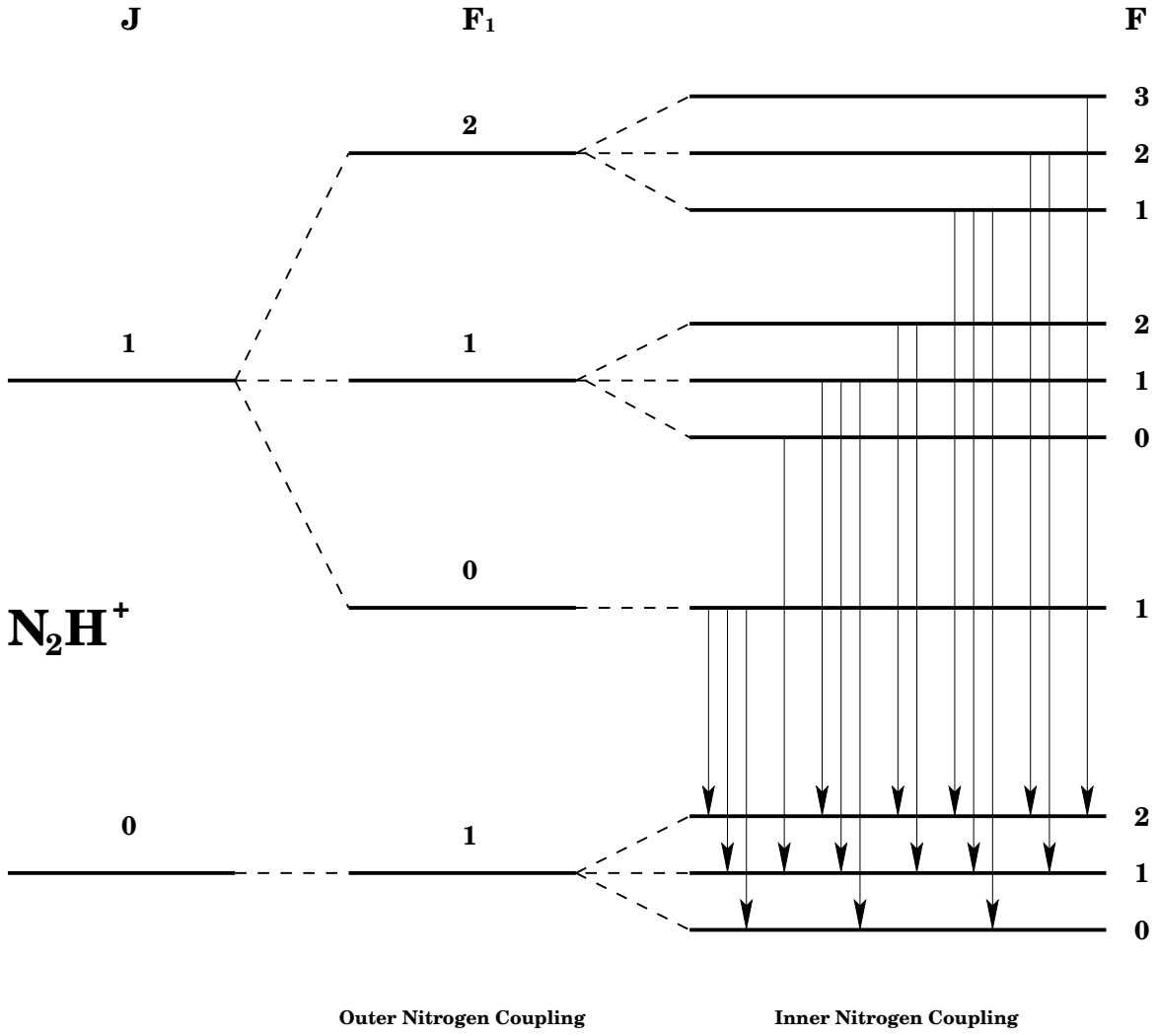

Fig. 5.— Energy level structure for the $J = 1 \rightarrow 0$ transition of N_2H^+. Note that of the 15 hyperfine split levels only 7 are observed due to the fact that the hyperfine splitting of the J=0 level is very small. Grouping of the indicated transitions show the 7 observed transitions. Transitions are ordered by increasing frequency from left to right.

Table 7. Outer Nitrogen (F_1) Hyperfine Intensities for N_2H^+ $J = 1 \rightarrow 0$

$F_1' \rightarrow F_1$ [a]	$J' \rightarrow J$ [a]	a	b	c	Type	$\frac{(2F_1'+1)(2F_1+1)}{(2I+1)}$	6j	$R_i(F_1, J)$
(0,1)	(1,0)	1	0	1	3	1	$\frac{1}{3}$	$\frac{1}{9}$
(1,1)	(1,0)	1	1	1	2	3	$-\frac{1}{3}$	$\frac{1}{3}$
(2,1)	(1,0)	1	1	2	1	5	$\frac{1}{3}$	$\frac{5}{9}$

[a] $Z = F_1$ and $X = J$.

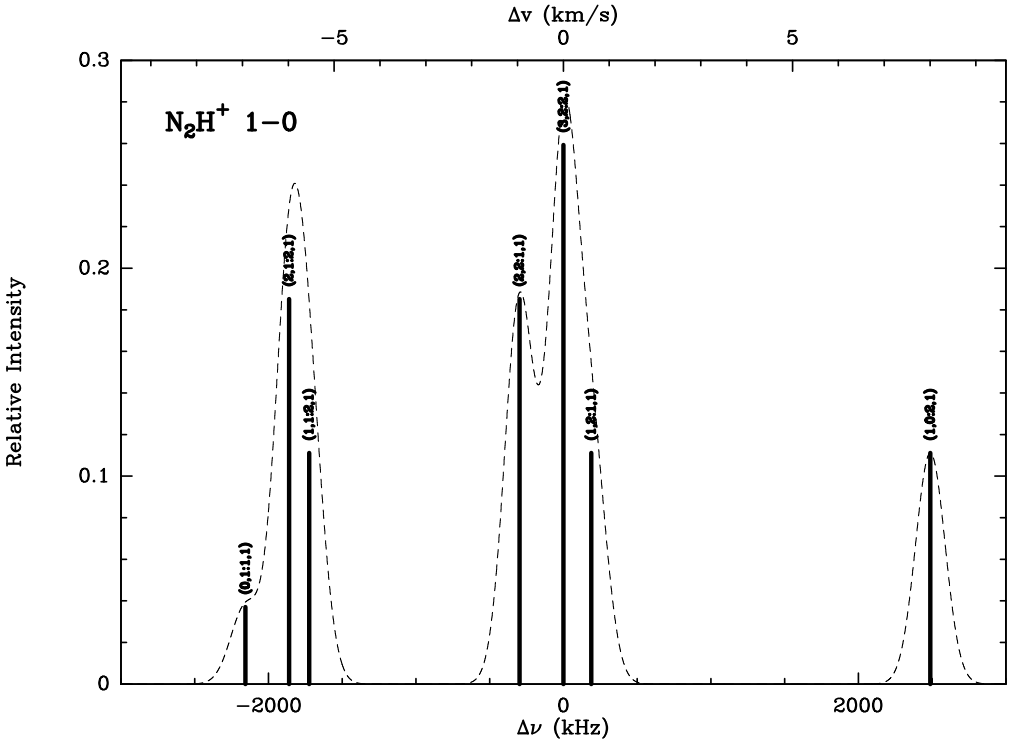

Fig. 6.— Synthetic spectra for the N_2H^+ $J = 1 \rightarrow 0$ transition. Horizontal axes are offset velocity (top) and frequency (bottom) relative to 93173776.7 kHz. Transition designations in (F',F_1':F,F_1) format are indicated. Overlain in dash is a synthetic 100 kHz gaussian linewidth source spectrum.

Table 8. Inner Nitrogen (F) Hyperfine Intensities for N_2H^+ $J = 1 \rightarrow 0$

$F' \rightarrow F$[a]	$F_1' \rightarrow F_1$[a]	a	b	c	Type	$\frac{(2F'+1)(2F+1)}{(2I+1)}$	6j	$R_i(F, F_1)$
(1,0)	(0,1)	1	0	1	3	1	$\frac{1}{3}$	$\frac{1}{9}$
(1,1)	(0,1)	1	1	1	2	3	$-\frac{1}{3}$	$\frac{1}{3}$
(1,2)	(0,1)	1	1	2	1	5	$\frac{1}{3}$	$\frac{5}{9}$
(0,1)	(1,1)	1	1	1	2	1	$\frac{1}{3}$	$\frac{1}{9}$
(1,0)	(1,1)	1	1	1	2	1	$-\frac{1}{3}$	$\frac{1}{9}$
(1,1)	(1,1)	1	1	1	4	3	$\frac{1}{6}$	$\frac{1}{12}$
(1,2)	(1,1)	1	1	2	2	5	$\frac{1}{6}$	$\frac{5}{36}$
(2,1)	(1,1)	1	1	2	2	5	$\frac{1}{6}$	$\frac{5}{36}$
(2,2)	(1,1)	1	2	1	4	$\frac{25}{3}$	$-\frac{1}{2\sqrt{5}}$	$\frac{5}{12}$
(1,0)	(2,1)	1	2	1	1	1	$\frac{1}{3}$	$\frac{1}{9}$
(1,1)	(2,1)	1	1	2	2	3	$\frac{1}{6}$	$\frac{1}{12}$
(1,2)	(2,1)	1	1	2	3	5	$\frac{1}{30}$	$\frac{1}{180}$
(2,1)	(2,1)	1	2	2	1	5	$-\frac{1}{2\sqrt{5}}$	$\frac{1}{4}$
(2,2)	(2,1)	1	2	2	2	$\frac{25}{3}$	$-\frac{1}{10}$	$\frac{1}{12}$
(3,2)	(2,1)	1	2	3	1	$\frac{35}{3}$	$\frac{1}{5}$	$\frac{7}{15}$

[a] $Z = F$ and $X = F_1$.

Table 9. Hyperfine Intensities[a] for N_2H^+ J=1 → 0

$F' \rightarrow F$[b]	$F_1' \rightarrow F_1$[b]	$J' \rightarrow J$	$R_i(F_1, J)R_i(F, F_1)$	$\Delta\nu$[b] (kHz)	R_i(obs)[c]
(0,1)	(1,1)	(1,0)	$\frac{1}{27}$	−2155.7	$\frac{1}{27}$
(2,2)	(1,1)	(1,0)	$\frac{5}{36}$	−1859.9	$\frac{5}{27}$
(2,1)	(1,1)	(1,0)	$\frac{5}{108}$		
(1,2)	(1,1)	(1,0)	$\frac{5}{108}$	−1723.4	$\frac{1}{9}$
(1,1)	(1,1)	(1,0)	$\frac{1}{36}$		
(1,0)	(1,1)	(1,0)	$\frac{1}{27}$		
(2,1)	(2,1)	(1,0)	$\frac{5}{36}$	−297.1	$\frac{5}{27}$
(2,2)	(2,1)	(1,0)	$\frac{5}{108}$		
(3,2)	(2,1)	(1,0)	$\frac{7}{27}$	+0.0	$\frac{7}{27}$
(1,1)	(2,1)	(1,0)	$\frac{5}{108}$	+189.9	$\frac{1}{9}$
(1,2)	(2,1)	(1,0)	$\frac{1}{324}$		
(1,0)	(2,1)	(1,0)	$\frac{5}{81}$		
(1,2)	(0,1)	(1,0)	$\frac{5}{81}$	+2488.3	$\frac{1}{9}$
(1,1)	(0,1)	(1,0)	$\frac{1}{27}$		
(1,0)	(0,1)	(1,0)	$\frac{1}{81}$		

[a]The sum of the relative intensities $\sum_i R_i = 1.0$.

[b]Frequency offset in kHz relative to 93173.7767 MHz (Caselli et al. 1995).

[c]Since the J=0 level splitting is very small, only the sum of all transitions into the J=0 is observed.

To derive the column density for N_2H^+ we start with the general equation for the total molecular column density (Equation 28) with:

$$\begin{aligned}
S &= \frac{J_u}{2J_u+1} \text{ (see §8.1)} \\
\mu &= 3.37 \text{ Debye} \\
B_0 &= 46586.88 \text{ MHz} \\
R_i &= \text{(see §10 or, for J=1-0, see Table 9)} \\
g_u &= 2J_u+1 \\
g_K &= 1 \text{ (for linear molecules)} \\
g_I &= 1 \text{ (for linear molecules)} \\
Q_{rot} &\simeq \frac{kT}{hB} + \frac{1}{3} (Equation\ 46) \\
&\simeq 0.45\,(T+0.74) \\
E_u &= 4.4716 \text{ K}
\end{aligned} \tag{84}$$

which leads to:

$$N_{tot}(N_2H^+) = \frac{3h}{8\pi^3\mu^2}\frac{Q_{rot}}{J_u R_i}\exp\left(\frac{E_u}{kT_{ex}}\right)\left[\exp\left(\frac{h\nu}{kT_{ex}}\right)-1\right]^{-1}\int \tau_\nu dv \tag{85}$$

Assuming optically thin emission and and $T_{bg} \ll T_{ex}$, we find that Equation 85 becomes:

$$N_{tot}(N_2H^+) = \frac{6.25\times10^{15}}{\nu(GHz)R_i}\exp\left(\frac{E_u}{kT_{ex}}\right)T_B\Delta v(km/s)\ \text{cm}^{-2} \tag{86}$$

where ν is the frequency of the hyperfine transition used. For example, if the F=(2,1), J=(1,0) hyperfine was chosen for this calcuation, $R_i = \frac{7}{27}$ (See Table 9) and $\nu = 93.1737767\,\text{GHz}$. Equation 86 then becomes:

$$N_{tot}(N_2H^+) = 2.59 \times 10^{14} \exp\left(\frac{E_u}{kT_{ex}}\right) T_B \Delta v(km/s) \text{ cm}^{-2} \quad (87)$$

12.4. NH_3

Ammonia (NH_3) is a symmetric top molecule with three opposing identical H (spin=$\frac{1}{2}$) nuclei. Quantum mechanical tunneling of the N nucleus through the potential plane formed by the H nuclei leads to inversion splitting of each NH_3 energy level. On top of this inversion splitting the energy levels are split due to two hyperfine interactions:

J–$\mathbf{I}_N$: Coupling between the quadrupole moment of the N nucleus and the electric field of the H atoms, which splits each energy level into three hyperfine states. For this interaction the angular momentum vectors are defined as follows: $\vec{F_1} = \vec{J} + \vec{I_N}$.

$\mathbf{F}_1$–$\mathbf{I}_H$: Coupling between the magnetic dipole of the three H nuclei with the weak current generated by the rotation of the molecule. For this interaction the angular momentum vectors are defined as follows: $\vec{F} = \vec{F_1} + \vec{I_H}$.

Weaker N-H spin-spin and H-H spin-spin interactions also exist, but only represent small perturbations of the existing hyperfine energy levels. Note too that "anomalies" between observed hyperfine transitions intensities and those predicted by quantum mechanics have been observed (see Stutzki et al. (1984) and Stutzki & Winnewisser (1985)). These anomalies are likely due to "line overlap" between the hyperfine transitions.

Figure 7 shows the rotational energy level diagram for the first three J-levels of NH_3, while Figure 8 shows the inversion and hyperfine level structure for the (1,1) transition. (ADD (3,3) and (4,4) AS TIME PERMITS.) Figure 9 shows all NH_3 energy levels below 600 K. Table 10 lists level energies.

Table 10. NH_3 Level Energies[a,b]

Level	Energy (K)	Level	Energy (K)
(0,0,a)	1.14	...	...
(1,1,s)	23.21	(1,1,a)	24.35
(1,0,s)	28.64	...	...
(2,2,s)	64.20	(2,2,a)	65.34
(2,1,s)	80.47	(2,1,a)	81.58
(2,0,a)	86.99	...	...
(3,3,s)	122.97	(3,3,a)	124.11
(3,2,s)	150.06	(3,2,a)	151.16
(3,1,s)	166.29	(3,1,a)	167.36
(3,0,s)	171.70	...	...
(4,4,s)	199.51	(4,4,a)	200.66
(4,3,s)	237.40	(4,3,a)	238.48
(4,2,s)	264.41	(4,2,a)	265.45
(4,1,s)	280.58	(4,1,a)	281.60
(4,0,a)	286.98	...	...
(5,5,s)	293.82	(5,5,a)	295.00
(5,4,s)	342.49	(5,4,a)	343.58
(5,3,s)	380.23	(5,3,a)	381.25
(5,2,s)	407.12	(5,2,s)	408.10
(5,1,s)	423.23	(5,1,a)	424.18
(5,0,s)	428.60	...	...
(6,6,s)	405.91	(6,6,a)	407.12
(6,3,s)	551.30	(6,3,a)	552.25
(6,0,a)	600.30	...	...

[a]isted in level energy order per J and inversion-paired as appropriate.

[b]See Poynter & Kakar (1975) for lower-state energy calculations.

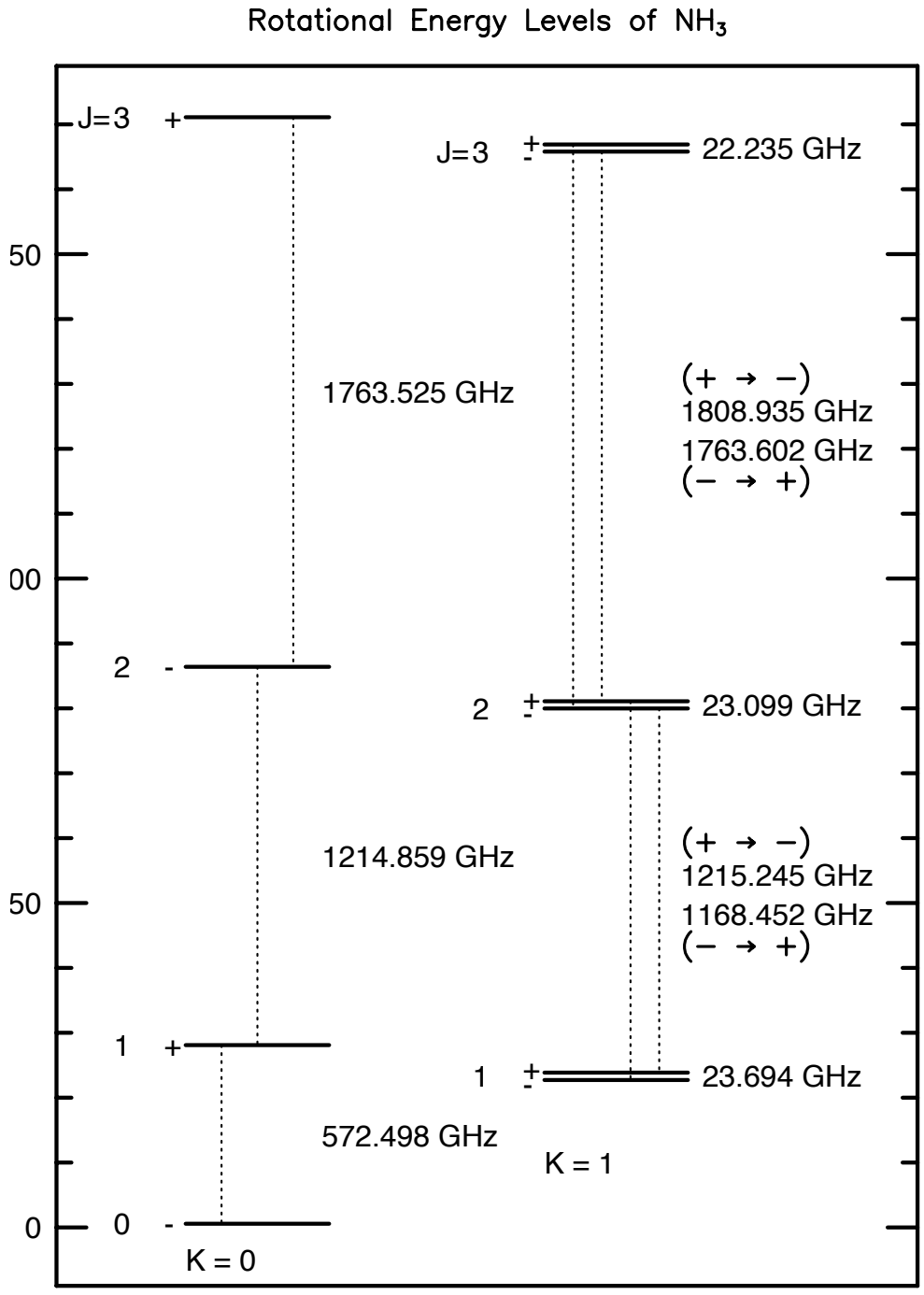

Fig. 7.— Rotational energy level diagram for the first three J-levels of NH_3.

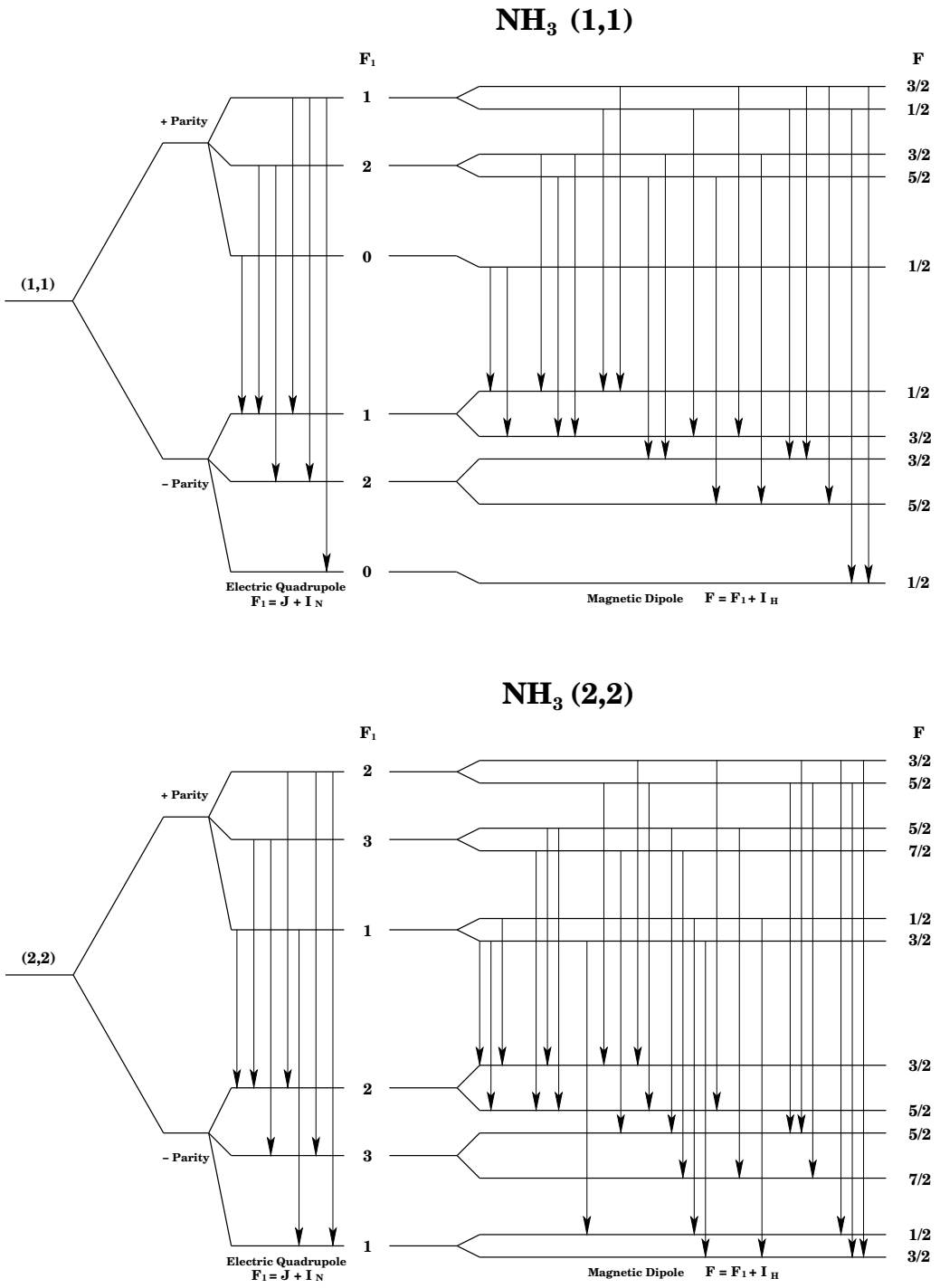

Fig. 8.— Inversion and hyperfine energy level structure for the (1,1) (top) and (2,2) (bottom) transitions of NH_3. Note that the 18 (1,1) and 24 (2,2) allowed transitions are marked with arrows ordered by increasing frequency from left to right. Adapted from Ho & Townes (1983).

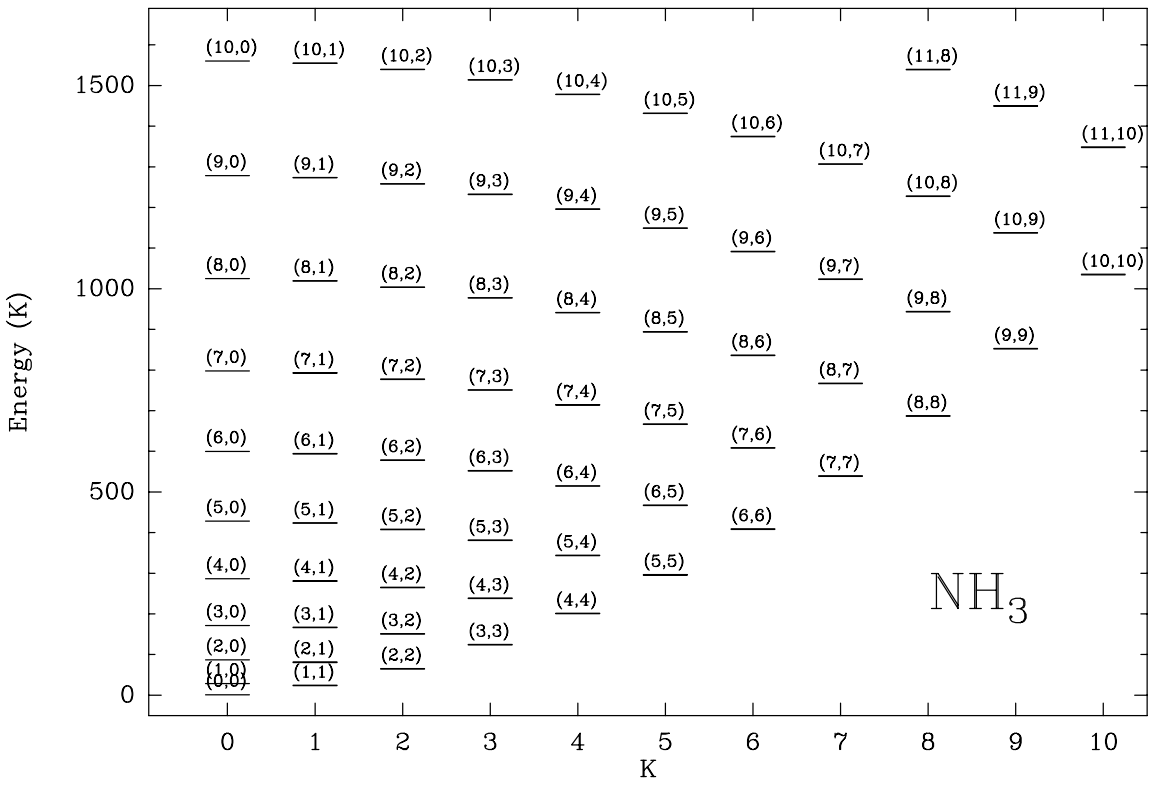

Fig. 9.— Rotational energy level diagram for NH_3. All levels with energy $< 1600\,\mathrm{K}$ are shown.

We can calculate the relative hyperfine intensities (R_i) for the (1,1) and (2,2) transitions using the formalism derived in §10. Using Table 4 we can derive the relevant R_i for the quadrupole hyperfine ($R_i(F_1, J)$, I=1; Tables 12, 13, 14, and 15) and magnetic hyperfine ($R_i(F, F_1)$, I=$\frac{1}{2}$; Tables 16 and 17) coupling cases. The resultant hyperfine intensities are listed in Tables 18 and 19 (add (3,K) and (4,K) when available). Note that in the appropriate tables we list the association between Z and X and their associated quantum numbers following the assignment mapping equations listed in Equation 67. Figure 10 shows the synthetic spectra for the NH_3 (1,1) and (2,2) transitions.

For illustration we can derive the column density equation for a para-NH_3 (K≠0 or 3n) inversion ($\Delta K = 0$) transition. For para-NH_3 inversion transitions:

$$
\begin{aligned}
S &= \frac{K^2}{J_u(J_u+1)} \\
\mu &= 1.468 \text{ Debye} \\
R_i &= \text{(see §10 or, for (1,1) and (2,2), see Tables 18 and 19)} \\
g_u &= 2J_u + 1 \\
g_K &= 2 \text{ for K}\neq 0 \\
g_I &= \frac{2}{8} \text{ for K}\neq 3\text{n}
\end{aligned}
$$

We can compute the following equation for the molecular column density in NH_3 as derived from a measurement of a (J,K) (K≠0 or 3n) inversion ($\Delta K = 0$) transition assuming:

- Summation over all hyperfine levels in a given (J,K) transition (note that $\sum_i R_i = 1$),
- Optically thin emission,
- Unity filling factor (f=1),

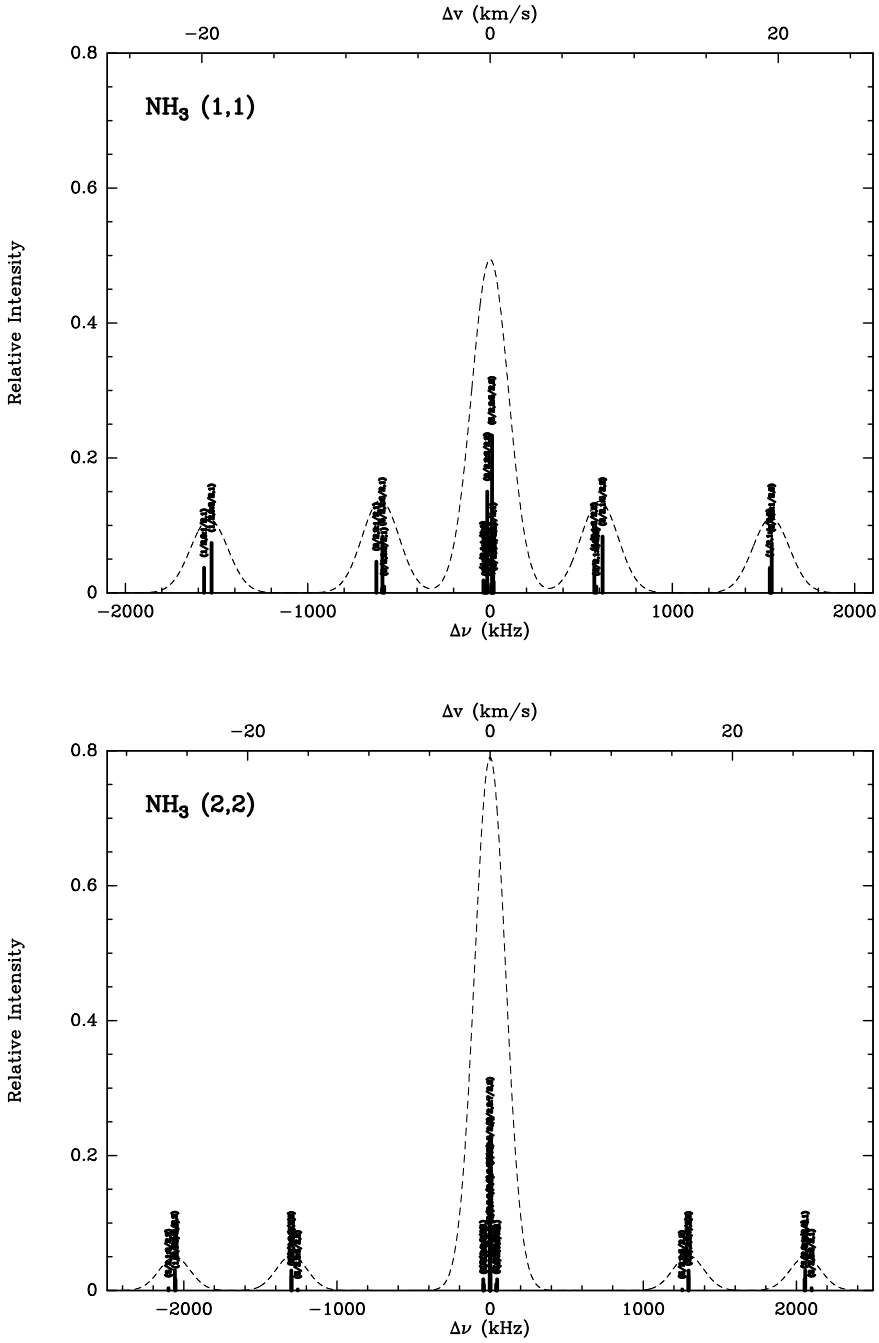

Fig. 10.— Synthetic spectra for the NH_3 (1,1) (top) and (2,2) (bottom) transitions. Horizontal axes are offset velocity (top) and frequency (bottom) relative to 23694495.487 and 23722633.335 kHz, respectively. Transition designations in (F',F_1':F,F_1) format are indicated. Overlain in dash is a synthetic 100 kHz gaussian linewidth source spectrum.

using Equation 74:

$$\begin{aligned} N_{tot}(NH_3) &= \frac{3k}{8\pi^3\mu^2 R_i}\frac{J_u(J_u+1)}{K^2}\frac{Q_{rot}}{g_u g_K g_I}\exp\left(\frac{E_u}{kT_{ex}}\right)\int T_R dv \\ &\simeq \frac{3.34\times10^{14}J_u(J_u+1)Q_{rot}}{\nu(GHz)\mu^2(Debye)K^2(2J_u+1)R_i}\exp\left(\frac{E_u}{kT_{ex}}\right)\int T_R dv(km/s)\ \mathrm{cm}^{-2} \\ &\simeq \frac{1.55\times10^{14}J_u(J_u+1)Q_{rot}}{\nu(GHz)K^2(2J_u+1)R_i}\exp\left(\frac{E_u}{kT_{ex}}\right)\int T_R dv(km/s)\ \mathrm{cm}^{-2} \end{aligned} \tag{88}$$

12.5. H_2CO

Formaldehyde (H_2CO) is a slightly asymmetric rotor molecule. The level of asymmetry in molecules is often described in terms of Ray's asymmetry parameter κ (Ray 1932):

$$\kappa \equiv \frac{2B-A-C}{A-C} \tag{89}$$

where A, B, and C are the rotational angular momentum constants for the molecule, usually expressed in MHz. For H_2CO, A = 281970.37 MHz, B = 38835.42558 MHz, and C = 34005.73031 MHz, which yields $\kappa \simeq -0.961$, which means that H_2CO is nearly a prolate symmetric rotor. The slight asymmetry in H_2CO results in limiting prolate (quantum number K_{-1}) and oblate (quantum number K_{+1}) symmetric rotor energy levels that are closely spaced in energy, a feature commonly referred to as "K-doublet splitting". Figure 11 shows the energy level diagram for H_2CO including all energy levels $E \leq 300$ K. In addition to the asymmetric rotor energy level structure H_2CO possess spin-rotation and spin-spin hyperfine energy level structure. Magnetic dipole interaction between the H nuclei and rotational motion of the molecule result in spin-rotation hyperfine energy level splitting. For the $1_{10}-1_{11}$ transition the frequency offsets of these hyperfine transitions are $\delta\nu \leq 18.5$ kHz. The weaker spin-spin interactions between the nuclei are generally not considered.

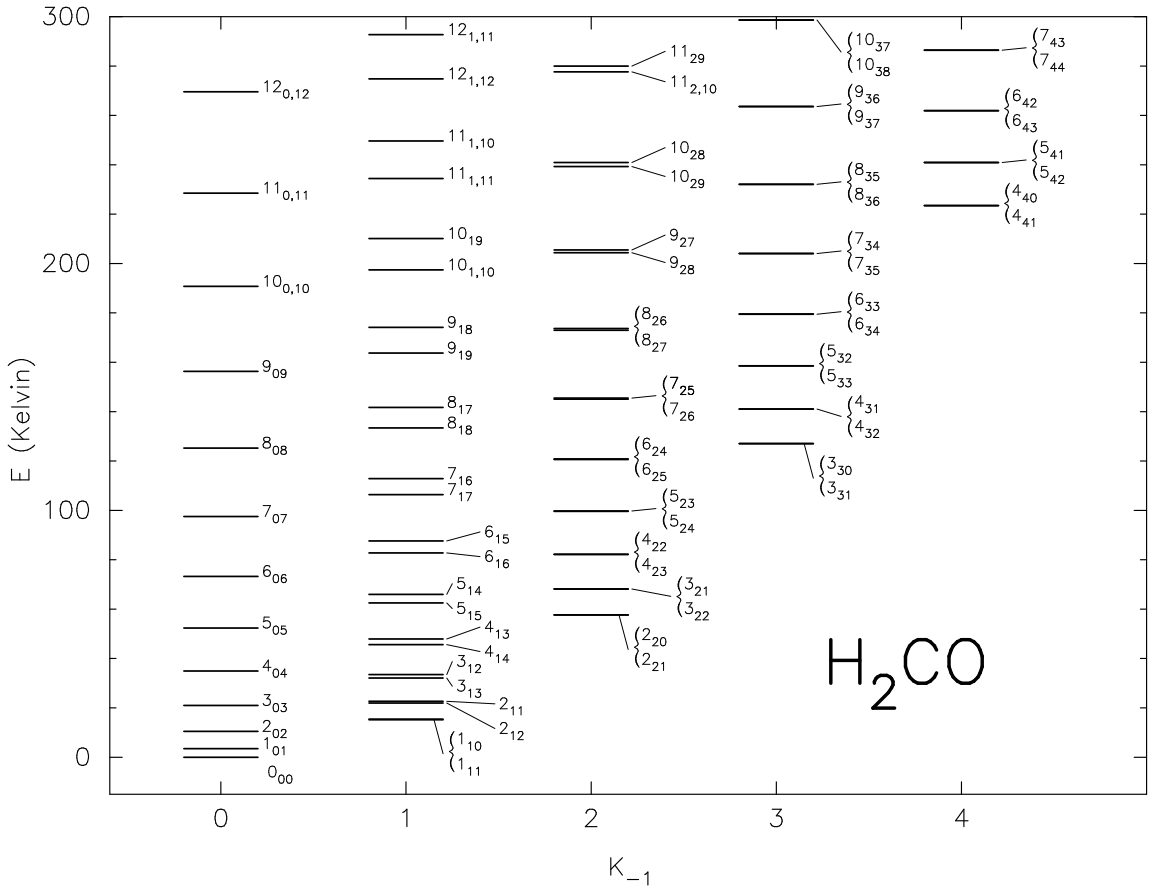

Fig. 11.— Energy level diagram for H_2CO including all energy levels with $E \leq 300\,\mathrm{K}$.

Table 11 lists the frequencies and relative intensities for the spin-rotation hyperfine transitions of the H_2CO $1_{10} - 1_{11}$, $2_{11} - 2_{12}$, and $3_{12} - 3_{13}$ transitions. Note that in Table 11 we list the association between Z and X and their associated quantum numbers following the assignment mapping equations listed in Equation 67. Figure 12 shows the synthetic spectra for the NH_3 (1,1) and (2,2) transitions. Furthermore, note that the hyperfine intensities are exactly equal to those calculated for the spin-rotation hyperfine components of NH_3 (see §E).

For illustration we can derive the column density equation for a ortho-H_2CO (K odd) K-doublet ($\Delta K = 0$) transition. For ortho-H_2CO transitions:

$$
\begin{aligned}
S &= \frac{K^2}{J_u(J_u+1)} \\
\mu &= 2.331 \text{ Debye} \\
R_i &= \text{(see §10 or, for } 1_{10} - 1_{11},\ 2_{11} - 2_{12}, \text{ or } 3_{12} - 3_{13} \text{ see Table 11)} \\
g_u &= 2J_u + 1 \\
g_K &= 2 \text{ for K} \neq 0 \\
g_I &= \frac{3}{4} \text{ for K odd}
\end{aligned}
$$

We can compute the following equation for the molecular column density in H_2CO as derived from a measurement of a (J,K) (K odd) K-doublet ($\Delta K = 0$) transition assuming:

- Summation over all hyperfine levels in a given (J,K) transition (note that $\sum_i R_i = 1$),
- Optically thin emission,
- Unity filling factor (f=1),

using Equation 74:

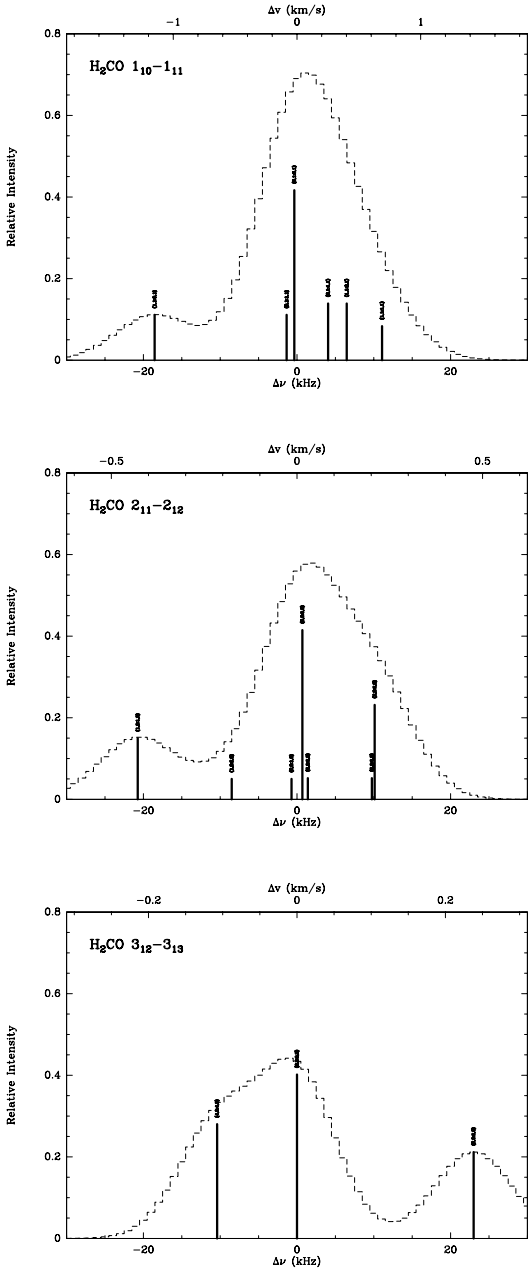

Fig. 12.— Synthetic spectra for the H_2CO $1_{10} - 1_{11}$, $2_{11} - 2_{12}$, and $3_{12} - 3_{13}$ transitions. Horizontal axes are offset velocity (top) and frequency (bottom) relative to blaaa, blaaa, and blaaa kHz, respectively. Transition designations in (F'_1,J′:F_1,J) format are indicated. For the $3_{12} - 3_{13}$ transition only the $\Delta F = 0$ hyperfine transitions are shown. Overlain in dash is a synthetic 10 kHz gaussian linewidth source spectrum.

Table 11. F_1-I_H Hyperfine Frequencies and Intensities for H_2CO J=1 − 1, 2 − 2, and 3 − 3 K-Doublet transitions

$F_1' \rightarrow F_1$[a]	$J' \rightarrow J$[a]	Δ_{HF}[b] (kHz)	a	b	c	Type	$\frac{(2F_1'+1)(2F_1+1)}{(2I+1)}$	6j	$R_i(F_1, J)$
(1,0)	(1,1)	−18.53	1	1	1	2	1	$-\frac{1}{3}$	$\frac{1}{9}$
(0,1)	(1,1)	−1.34	1	1	1	2	1	$-\frac{1}{3}$	$\frac{1}{9}$
(2,2)	(1,1)	−0.35	1	2	1	4	$\frac{25}{3}$	$-\frac{1}{2\sqrt{5}}$	$\frac{5}{12}$
(2,1)	(1,1)	+4.05	1	1	2	2	5	$\frac{1}{6}$	$\frac{5}{36}$
(1,2)	(1,1)	+6.48	1	1	2	2	5	$\frac{1}{6}$	$\frac{5}{36}$
(1,1)	(1,1)	+11.08	1	1	1	4	3	$\frac{1}{6}$	$\frac{1}{12}$
(1,1)	(2,2)	−20.73	1	1	2	4	3	$\frac{1}{2\sqrt{5}}$	$\frac{3}{20}$
(1,2)	(2,2)	−8.5	1	2	2	2	5	$-\frac{1}{10}$	$\frac{1}{20}$
(2,1)	(2,2)	−0.71	1	2	2	2	5	$-\frac{1}{10}$	$\frac{1}{20}$
(3,3)	(2,2)	+0.71	1	3	2	4	$\frac{49}{3}$	$-\frac{2\sqrt{2}}{3\sqrt{35}}$	$\frac{392}{945}$
(3,2)	(2,2)	+1.42	1	2	3	2	$\frac{35}{3}$	$\frac{1}{15}$	$\frac{7}{135}$
(2,3)	(2,2)	+9.76	1	2	3	2	$\frac{35}{3}$	$\frac{1}{15}$	$\frac{7}{135}$
(2,2)	(2,2)	+10.12	1	2	2	4	$\frac{25}{3}$	$\frac{1}{6}$	$\frac{25}{108}$
(2,3)	(3,3)	...	1	3	3	2	$\frac{35}{3}$	$-\frac{1}{21}$	$\frac{5}{189}$
(4,3)	(3,3)	...	1	3	4	2	21	$\frac{1}{28}$	$\frac{3}{112}$
(4,4)	(3,3)	+0.00	1	4	3	4	27	$-\frac{\sqrt{5}}{4\sqrt{21}}$	$\frac{45}{112}$
(3,3)	(3,3)	−10.4	1	3	3	4	$\frac{49}{3}$	$\frac{11}{84}$	$\frac{121}{432}$
(2,2)	(3,3)	+23.0	1	2	3	4	$\frac{25}{3}$	$\frac{-2\sqrt{2}}{3\sqrt{35}}$	$\frac{40}{189}$
(3,4)	(3,3)	...	1	3	4	2	21	$\frac{1}{28}$	$\frac{3}{112}$
(3,2)	(3,3)	...	1	3	3	2	$\frac{35}{3}$	$-\frac{1}{21}$	$\frac{5}{189}$

[a] $Z = F_1$ and $X = J$.

[b] Frequency offset in kHz relative to 4829.6596 MHz for $1_{10} - 1_{11}$, 14488.65 MHz for $2_{11} - 2_{12}$, and 28974.85 MHz for $3_{12} - 3_{13}$.

$$
\begin{aligned}
N_{tot}(H_2CO) &= \frac{3k}{8\pi^3\mu^2 R_i}\frac{J_u(J_u+1)}{K^2}\frac{Q_{rot}}{g_u g_K g_I}\exp\left(\frac{E_u}{kT_{ex}}\right)\int T_R dv \\
&\simeq \frac{1.11\times 10^{14} J_u(J_u+1)Q_{rot}}{\nu(GHz)\mu^2(Debye)K^2(2J_u+1)R_i}\exp\left(\frac{E_u}{kT_{ex}}\right)\int T_R dv(km/s)\ \mathrm{cm}^{-2} \\
&\simeq \frac{2.04\times 10^{13} J_u(J_u+1)Q_{rot}}{\nu(GHz)K^2(2J_u+1)R_i}\exp\left(\frac{E_u}{kT_{ex}}\right)\int T_R dv(km/s)\ \mathrm{cm}^{-2} \qquad (90)
\end{aligned}
$$

REFERENCES

Caselli, P., Myers, P. C., & Thaddeus, P. 1995, ApJ, 455, L77

Cross, P. C., Hainer, R. M., & King, G. C. 1944, Journal of Chemical Physics, 12, 210

Draine, B. T. 2011, Physics of the Interstellar and Intergalactic Medium (Physics of the Interstellar and Intergalactic Medium by Bruce T. Draine. Princeton University Press, 2011. ISBN: 978-0-691-12214-4)

Edmonds, A. R. 1960, Angular Momentum in Quantum Mechanics (Angular Momentum in Quantum Mechanics, Princeton: Princeton University Press, 1960)

Gordy, W., & Cook, R. L. 1984, Microwave Molecular Spectra (Microwave Molecular Spectra, New York: Interscience Pub., 1970)

Harris, A. I., Baker, A. J., Zonak, S. G., et al. 2010, ApJ, 723, 1139

Ho, P. T. P., & Townes, C. H. 1983, ARA&A, 21, 239

Jennings, D. A., Evenson, K. M., Zink, L. R., et al. 1987, Journal of Molecular Spectroscopy, 122, 477

Kukolich, S. G. 1967, Phys. Rev., 156, 83

Mangum, J. G., Wootten, A., & Mundy, L. G. 1992, ApJ, 388, 467

McDowell, R. S. 1988, Journal of Chemical Physics, 88, 356

—. 1990, Journal of Chemical Physics, 93, 2801

Poynter, R. L., & Kakar, R. K. 1975, ApJS, 29, 87

Ray, R. S. 1932, Zeitschrift für Physik, 78, 74

Shirley, Y. L., Nordhaus, M. K., Grcevich, J. M., et al. 2005, ApJ, 632, 982

Spitzer, L. 1978, Physical processes in the interstellar medium (New York Wiley-Interscience, 1978. 333 p.)

Stutzki, J., Olberg, M., Winnewisser, G., Jackson, J. M., & Barrett, A. H. 1984, A&A, 139, 258

Stutzki, J., & Winnewisser, G. 1985, A&A, 144, 13

Tatum, J. B. 1986, ApJS, 60, 433

Turner, B. E. 1991, ApJS, 76, 617

Ulich, B. L., & Haas, R. W. 1976, ApJS, 30, 247

A. Line Profile Functions

For a Gaussian profile the function $\phi(\nu)$ is given by

$$\phi(\nu) = \frac{1}{\sqrt{2\pi}\sigma} \exp\left[-\frac{(\nu-\nu_0)^2}{2\sigma^2}\right] \tag{A1}$$

where

$$2\sigma^2 = \frac{\nu_0^2}{c^2}\left(\frac{2kT_k}{M} + v^2\right) \tag{A2}$$

and

This manuscript was prepared with the AAS LaTeX macros v5.2.

$$\int \phi(\nu) d\nu = 1 \tag{A3}$$

The Gaussian profile has a FWHM given by (in both frequency and velocity):

$$\Delta\nu_D = \frac{2\nu_0}{c}\left[\ln 2\left(\frac{2kT_k}{M} + v^2\right)\right]^2 \tag{A4}$$

$$\Delta v_D = 2\left[\ln 2\left(\frac{2kT_k}{M} + v^2\right)\right]^2 \tag{A5}$$

and a peak value given by:

$$\phi(\nu)_{peak} = \frac{2\sqrt{\ln 2}}{\sqrt{\pi}\Delta\nu_D} \tag{A6}$$

$$= \frac{2\sqrt{\ln 2}c}{\sqrt{\pi}\nu_0\Delta v_D} \tag{A7}$$

If one uses peak values instead of integrating over a Gaussian profile to derive column densities, one must make the following correction:

$$(N_{tot})_{Gauss} = 2\sqrt{\frac{\ln 2}{\pi}}(N_{tot})_{peak} \tag{A8}$$

B. Integrated Fluxes Versus Brightness Temperatures

All calculations in this document assume the use of integrated brightness temperatures ($\int T_B \Delta v$). If one uses integrated fluxes ($\int S_\nu \Delta v$), the total molecular column density assuming optically-thin emission (Equation 74) is modified by using the relationship between flux density and brightness temperature:

$$S_\nu = \frac{2kT_B\nu^2}{c^2}\Omega_s \tag{B1}$$

and becomes

$$N_{tot} = \left(\frac{D}{2R_s}\right)^2 \frac{3c^2}{16\pi^3 S\mu^2\nu^3}\left(\frac{Q_{rot}}{g_u g_K g_{nuclear}}\right)\exp\left(\frac{E_u}{kT}\right)\int S_\nu \Delta v \tag{B2}$$

$$= \frac{3c^2}{16\pi^3\Omega_s S\mu^2\nu^3}\left(\frac{Q_{rot}}{g_u g_K g_{nuclear}}\right)\exp\left(\frac{E_u}{kT}\right)\int S_\nu \Delta v \tag{B3}$$

C. Integrated Intensity Uncertainty

For cases where you do not have a calculation from a fit to the integrated intensity of a spectral line, one can use the following estimate given a measurement of the baseline RMS and line profile properties.

$$\int T dv = \Delta v_c \sum_{n=1}^{N} T_n \equiv I \tag{C1}$$

...where Δv_c is the spectral velocity channel width, T_n is a spectral channel value, and the line spans N channels. The statistical uncertainty of the integrated line intensity is given by:

$$\sigma_I^2 = \sigma_T^2\left[\frac{\partial I}{\partial T}\right]^2 + \sigma_{\Delta v_c}^2\left[\frac{\partial I}{\partial(\Delta v_c)}\right]^2 \tag{C2}$$

$$= \sigma_T^2(\Delta v_c)^2 \tag{C3}$$

...where I have used the fact that we know the velocity channel width ($\sigma_{\Delta v_c} = 0$). Using Equation C2 in Equation C3, and assuming that all of the channel noise values are equal:

$$\sum_{n=1}^{N} \sigma_{T_n}^2 = N\sigma_T^2 \tag{C4}$$

...we get...

$$\sigma_I^2 = N\sigma_T^2(\Delta v_c)^2 \tag{C5}$$

$$\sigma_I = \sqrt{N}\sigma_T \Delta v_c \tag{C6}$$

$$= \sqrt{\Delta v_{line} \Delta v_c}\sigma_T \tag{C7}$$

...where we have used the fact that the spectral line width $\Delta v_{line} = N\Delta v_c$ to get the last expression for σ_I.

D. Excitation and Kinetic Temperature

This section is drawn from Appendix A of Mangum et al. (1992). If the metastable states in NH_3 are coupled only through collisions and the populations in the upper states in each K–ladder (J≠K) can be neglected, the populations in the metastable states are related through the Boltzmann equation. In molecular clouds, though, ΔK = 1 collisions across K–ladders will deplete metastable states in favor of their next lower J metastable states. Therefore, for example, collisional de–excitation of the (2,2) transition will result in an increase in the population of the (2,1) state, followed by quick radiative relaxation of the (2,1) state into the (1,1) state. This implies that an excitation temperature, $T_{ex}(J', K'; J, K)$ relating the populations in the (J′,K′) and (J,K) states, n(J′,K′) and n(J,K), may be derived. From the Boltzmann equation,

$$\frac{n(J',K')}{n(J,K)} = \frac{g(J',K')}{g(J,K)} \exp\left[-\frac{\Delta E(J',K';J,K)}{T_{ex}(J',K';J,K)}\right] \tag{D1}$$

and the ratio of level (J′,K′) and (J,K) column densities (assuming $h\nu \ll kT_{ex}(J',K';J,K)$) for the (J,K) and (J′,K′) transitions

$$\frac{N(J',K')}{N(J,K)} = \frac{J'(J'+1)K^2\tau(J',K')\Delta v(J',K')}{J(J+1)(K')^2\tau(J,K)\Delta v(J,K)} \tag{D2}$$

and the fact that in a homogeneous molecular cloud

$$\frac{n(J',K')}{n(J,K)} = \frac{N(J',K')}{N(J,K)} \tag{D3}$$

we find that

$$\frac{g(J',K')}{g(J,K)} \exp\left[-\frac{\Delta E(J',K';J,K)}{T_{ex}(J',K';J,K)}\right] = \frac{J'(J'+1)K^2\tau(J',K')\Delta v(J',K')}{J(J+1)(K')^2\tau(J,K)\Delta v(J,K)} \tag{D4}$$

Using

$$\tau(J,K) = \left[\sum^{F,F'} R_{F,F'} / \sum^{F,F'} R_m\right] \tau(J,K,m) \tag{D5}$$

where R is the relative intensity for a quadrupole (F,F_1) or main (m) hyperfine component and

$$
\begin{aligned}
I_{JK} &\equiv \left[\sum^{F,F'} R_{F,F'} / \sum^{F,F'} R_m\right] \\
&= \frac{1.0}{\frac{5}{12}+\frac{1}{12}} \\
&= 2.000 \text{ for the (1,1) transition (see Tables 12 or 18)} \\
&= \frac{1.0}{\frac{56}{135}+\frac{25}{108}+\frac{3}{20}} \\
&= 1.256 \text{ for the (2,K) transitions (see Tables 13 or 19)} \\
&= \frac{54}{43} \\
&= \frac{1.0}{\frac{45}{112}+\frac{121}{432}+\frac{40}{189}} \\
&= \frac{216}{193} \\
&= 1.119 \text{ for the (3,K) transitions (see Table 14)} \\
&= \frac{1.0}{\frac{968}{2475}+\frac{361}{1200}+\frac{35}{144}} \\
&= \frac{2200}{2057} \\
&= 1.070 \text{ for the (4,K) transitions (see Table 15)}
\end{aligned}
$$

for the (1,1) and (2,2) transitions, we can relate the total optical depth τ(J,K) to the optical depth in the main hyperfine component τ(J,K,m), noting that for NH_3 g(J,K) = $2J_u + 1$, and solving Equation D4 for $T_{ex}(J', K'; J, K)$ we find that

$$
\begin{aligned}
T_{ex}(J', K'; J, K) &= -\Delta E(J', K'; J, K) \\
&\quad \left\{\ln\left[\frac{(2J+1)J'(J'+1)K^2 I_{J'K'}\tau(J', K', m)\Delta v(J', K')}{(2J'+1)J(J+1)(K')^2 I_{JK}\tau(J, K, m)\Delta v(J, K)}\right]\right\}^{-1} \quad \text{(D6)}
\end{aligned}
$$

Using

$$\frac{T_B(J,K,m)}{T_B(J',K',m)} = \frac{1-\exp\left[-\tau(J,K,m)\right]}{1-\exp\left[-\tau(J',K',m)\right]} \tag{D7}$$

which assumes equal excitation temperatures and beam filling factors in the (J,K) and (J′,K′) transitions. Solving Equation D7 for $\tau(J',K',m)$ yields

$$\tau(J',K',m) = -\ln\left[1-\frac{T_B(J',K',m)}{T_B(J,K,m)}\left\{1-\exp\left[-\tau(J,K,m)\right]\right\}\right] \tag{D8}$$

Substituting Equation D8 into Equation D6

$$\begin{aligned} T_{ex}(J',K';J,K) = &-\Delta E(J',K';J,K) \\ &\times\left\{\ln\left[\frac{(2J+1)J'(J'+1)K^2 I_{J'K'}\Delta v(J',K')}{(2J'+1)J(J+1)(K')^2 I_{JK}\tau(J,K,m)\Delta v(J,K)}\right.\right. \\ &\left.\left.\times\ln\left(1-\frac{T_B(J',K',m)}{T_B(J,K,m)}\left\{1-\exp\left[-\tau(J,K,m)\right]\right\}\right)\right]\right\}^{-1} \end{aligned} \tag{D9}$$

For (J′,K′) = (2,2) and (J,K) = (1,1), Equation D9 becomes

$$\begin{aligned} T_{ex}(2,2;1,1) = -41.5\Bigg\{&\ln\Bigg[-\frac{0.283\Delta v(2,2)}{\tau(1,1,m)\Delta v(1,1)} \\ &\times\ln\left(1-\frac{T_B(2,2,m)}{T_B(1,1,m)}\left\{1-\exp\left[-\tau(1,1,m)\right]\right\}\right)\Bigg]\Bigg\}^{-1} \end{aligned} \tag{D10}$$

To derive the gas kinetic temperature from $T_{ex}(2,2;1,1)$, one uses statistical equilibrium (noting that only collisional processes are allowed between the different K–ladders), detailed balance, and the Boltzmann equation to calculate T_K from $T_{ex}(J',K';J,K)$. Assuming that the populations in the (1,1) and (2,2) transitions are much greater than that in the

higher lying levels of para–NH_3 and that the population of the non–metastable (2,1) level is negligible in comparison to that in the (1,1) level, we can use this "three–level model" of NH_3 to analytically derive an expression relating $T_{ex}(2,2;1,1)$ and T_K

$$1 + \frac{C(2,2;2,1)}{C(2,2;1,1)} = \left\{ \frac{g(1,1)}{g(2,2)} \exp\left[\frac{\Delta E(2,2;1,1)}{T_{ex}(2,2;1,1)} \right] \right\} \left\{ \frac{g(2,2)}{g(1,1)} \exp\left[-\frac{\Delta E(2,2;1,1)}{T_K} \right] \right\} \quad \text{(D11)}$$

where $C(J', K'; J, K)$ is the collisional excitation rate at temperature T_K between levels (J′,K′) and (J,K). Equation D11 can be re–written as

$$T_{ex}(2,2;1,1) \left\{ 1 + \left(\frac{T_K}{41.5} \right) \ln\left[1 + \frac{C(2,2;2,1)}{C(2,2;1,1)} \right] \right\} - T_K = 0 \quad \text{(D12)}$$

Solutions of Equation D12 give T_K for a measured $T_{ex}(2,2;1,1)$.

E. NH_3 Frequency and Relative Intensity Calculation Tables

Table 12. J–I_N Hyperfine Intensities for NH_3(1,1)

$F_1' \rightarrow F_1$[a]	$J' \rightarrow J$[a]	a	b	c	Type	$\frac{(2F_1'+1)(2F_1+1)}{(2I+1)}$	6j	$R_i(F_1, J)$
(0,1)	(1,1)	1	1	1	2	1	$-\frac{1}{3}$	$\frac{1}{9}$
(2,1)	(1,1)	1	1	2	2	5	$\frac{1}{6}$	$\frac{5}{36}$
(2,2)	(1,1)	1	2	1	4	$\frac{25}{3}$	$-\frac{1}{2\sqrt{5}}$	$\frac{5}{12}$
(1,1)	(1,1)	1	1	1	4	3	$\frac{1}{6}$	$\frac{1}{12}$
(1,2)	(1,1)	1	1	2	2	5	$\frac{1}{6}$	$\frac{5}{36}$
(1,0)	(1,1)	1	1	1	2	1	$-\frac{1}{3}$	$\frac{1}{9}$

[a] $Z = F_1$ and $X = J$.

Table 13. J–I_N Hyperfine Intensities for NH_3(2,K)

$F_1' \rightarrow F_1$[a]	$J' \rightarrow J$[a]	a	b	c	Type	$\frac{(2F_1'+1)(2F_1+1)}{(2I+1)}$	6j	$R_i(F_1, J)$
(1,2)	(2,2)	1	2	2	2	5	$-\frac{1}{10}$	$\frac{1}{20}$
(3,2)	(2,2)	1	2	3	2	$\frac{35}{3}$	$\frac{1}{15}$	$\frac{7}{135}$
(3,3)	(2,2)	1	3	2	4	$\frac{49}{3}$	$-\frac{2\sqrt{2}}{3\sqrt{35}}$	$\frac{56}{135}$
(2,2)	(2,2)	1	2	2	4	$\frac{25}{3}$	$\frac{1}{6}$	$\frac{25}{108}$
(1,1)	(2,2)	1	1	2	4	3	$-\frac{1}{2\sqrt{5}}$	$\frac{3}{20}$
(2,3)	(2,2)	1	2	3	2	$\frac{35}{3}$	$\frac{1}{15}$	$\frac{7}{135}$
(2,1)	(2,2)	1	2	2	2	5	$-\frac{1}{10}$	$\frac{1}{20}$

[a] $Z = F_1$ and $X = J$.

Table 14. J–I_N Hyperfine Intensities for NH_3(3,K)

$F_1' \rightarrow F_1$[a]	$J' \rightarrow J$[a]	a	b	c	Type	$\frac{(2F_1'+1)(2F_1+1)}{(2I+1)}$	6j	$R_i(F_1, J)$
(2,3)	(3,3)	1	3	3	2	$\frac{35}{3}$	$-\frac{1}{21}$	$\frac{5}{189}$
(4,3)	(3,3)	1	3	4	2	21	$\frac{1}{28}$	$\frac{3}{112}$
(4,4)	(3,3)	1	4	3	4	27	$-\frac{\sqrt{5}}{4\sqrt{21}}$	$\frac{45}{112}$
(3,3)	(3,3)	1	3	3	4	$\frac{49}{3}$	$\frac{11}{84}$	$\frac{121}{432}$
(2,2)	(3,3)	1	2	3	4	$\frac{25}{3}$	$-\frac{2\sqrt{2}}{3\sqrt{35}}$	$\frac{40}{189}$
(3,4)	(3,3)	1	3	4	2	21	$\frac{1}{28}$	$\frac{3}{112}$
(3,2)	(3,3)	1	3	3	2	$\frac{35}{3}$	$-\frac{1}{21}$	$\frac{5}{189}$

[a] $Z = F_1$ and $X = J$.

Table 15. J–I_N Hyperfine Intensities for NH_3(4,K)

$F_1' \rightarrow F_1$[a]	$J' \rightarrow J$[a]	a	b	c	Type	$\frac{(2F_1'+1)(2F_1+1)}{(2I+1)}$	6j	$R_i(F_1, J)$
(3,4)	(4,4)	1	4	4	2	21	$-\frac{1}{36}$	$\frac{7}{432}$
(5,4)	(4,4)	1	4	5	2	33	$\frac{1}{45}$	$\frac{11}{675}$
(5,5)	(4,4)	1	5	4	4	$\frac{121}{3}$	$-\frac{2\sqrt{2}}{5\sqrt{33}}$	$\frac{968}{2475}$
(4,4)	(4,4)	1	4	4	4	27	$\frac{19}{180}$	$\frac{361}{1200}$
(3,3)	(4,4)	1	3	4	4	$\frac{49}{3}$	$-\frac{\sqrt{5}}{4\sqrt{21}}$	$\frac{35}{144}$
(4,5)	(4,4)	1	4	5	2	33	$\frac{1}{45}$	$\frac{11}{675}$
(4,3)	(4,4)	1	4	4	2	21	$-\frac{1}{36}$	$\frac{7}{432}$

[a] $Z = F_1$ and $X = J$.

Table 16. F_1–I_H Hyperfine Frequencies and Intensities for NH_3(1,1)

$F' \rightarrow F$[a]	$F_1' \rightarrow F_1$[a]	$\Delta\nu_{HF}$[b] (kHz)	a	b	c	Type	$\frac{(2F'+1)(2F+1)}{(2I+1)}$	6j	$R_i(F, F_1)$
$(\frac{1}{2}, \frac{1}{2})$	(0,1)	−1568.487	$\frac{1}{2}$	$\frac{1}{2}$	1	2	2	$\frac{1}{\sqrt{6}}$	$\frac{1}{3}$
$(\frac{1}{2}, \frac{3}{2})$	(0,1)	−1526.950	$\frac{1}{2}$	1	$\frac{3}{2}$	1	4	$-\frac{1}{\sqrt{6}}$	$\frac{2}{3}$
$(\frac{3}{2}, \frac{1}{2})$	(2,1)	−623.306	$\frac{1}{2}$	2	$\frac{3}{2}$	1	4	$\frac{2}{\sqrt{3}}$	$\frac{1}{3}$
$(\frac{5}{2}, \frac{3}{2})$	(2,1)	−590.338	$\frac{1}{2}$	2	$\frac{5}{2}$	1	12	$-\frac{1}{2\sqrt{5}}$	$\frac{3}{5}$
$(\frac{3}{2}, \frac{3}{2})$	(2,1)	−580.921	$\frac{1}{2}$	$\frac{3}{2}$	2	2	8	$\frac{1}{2\sqrt{30}}$	$\frac{1}{15}$
$(\frac{1}{2}, \frac{1}{2})$	(1,1)	−36.536	$\frac{1}{2}$	$\frac{1}{2}$	1	4	2	$-\frac{1}{3}$	$\frac{2}{9}$
$(\frac{3}{2}, \frac{1}{2})$	(1,1)	−25.538	$\frac{1}{2}$	1	$\frac{3}{2}$	2	4	$-\frac{1}{6}$	$\frac{1}{9}$
$(\frac{5}{2}, \frac{3}{2})$	(2,2)	−24.394	$\frac{1}{2}$	2	$\frac{5}{2}$	2	12	$-\frac{1}{10\sqrt{3}}$	$\frac{1}{25}$
$(\frac{3}{2}, \frac{3}{2})$	(2,2)	−14.977	$\frac{1}{2}$	$\frac{3}{2}$	2	4	8	$-\frac{3}{10\sqrt{2}}$	$\frac{18}{50}$
$(\frac{1}{2}, \frac{3}{2})$	(1,1)	+5.848	$\frac{1}{2}$	1	$\frac{3}{2}$	2	4	$-\frac{1}{6}$	$\frac{1}{9}$
$(\frac{5}{2}, \frac{5}{2})$	(2,2)	+10.515	$\frac{1}{2}$	$\frac{5}{2}$	2	4	18	$\frac{\sqrt{7}}{15}$	$\frac{14}{25}$
$(\frac{3}{2}, \frac{3}{2})$	(1,1)	+16.847	$\frac{1}{2}$	$\frac{3}{2}$	1	4	8	$\frac{\sqrt{5}}{6\sqrt{2}}$	$\frac{5}{9}$
$(\frac{3}{2}, \frac{5}{2})$	(2,2)	+19.932	$\frac{1}{2}$	2	$\frac{5}{2}$	2	12	$-\frac{1}{10\sqrt{3}}$	$\frac{1}{25}$
$(\frac{1}{2}, \frac{3}{2})$	(1,2)	+571.792	$\frac{1}{2}$	2	$\frac{3}{2}$	1	4	$\frac{1}{2\sqrt{3}}$	$\frac{1}{3}$
$(\frac{3}{2}, \frac{3}{2})$	(1,2)	+582.790	$\frac{1}{2}$	$\frac{3}{2}$	2	2	8	$\frac{1}{2\sqrt{30}}$	$\frac{1}{15}$
$(\frac{3}{2}, \frac{5}{2})$	(1,2)	+617.700	$\frac{1}{2}$	2	$\frac{5}{2}$	1	12	$-\frac{1}{2\sqrt{5}}$	$\frac{3}{5}$
$(\frac{1}{2}, \frac{1}{2})$	(1,0)	+1534.050	$\frac{1}{2}$	$\frac{1}{2}$	1	2	2	$\frac{1}{\sqrt{6}}$	$\frac{1}{3}$
$(\frac{3}{2}, \frac{1}{2})$	(1,0)	+1545.049	$\frac{1}{2}$	1	$\frac{3}{2}$	1	4	$-\frac{1}{\sqrt{6}}$	$\frac{2}{3}$

[a] $Z = F$ and $X = F_1$.

[b] Frequency offset in kHz relative to 23694.495487 kHz (Kukolich 1967, Table I).

Table 17. F_1–I_H Hyperfine Frequencies and Intensities for $NH_3(2,2)$

$F' \rightarrow F$[a]	$F_1' \rightarrow F_1$[a]	$\Delta\nu_{HF}$[b] (kHz)	a	b	c	Type	$\frac{(2F'+1)(2F+1)}{(2I+1)}$	6j	$R_i(F,F_1)$
$(\frac{3}{2},\frac{3}{2})$	(1,2)	−2099.027	$\frac{1}{2}$	$\frac{3}{2}$	2	2	8	$\frac{1}{2\sqrt{30}}$	$\frac{1}{15}$
$(\frac{3}{2},\frac{5}{2})$	(1,2)	−2058.265	$\frac{1}{2}$	2	$\frac{5}{2}$	1	12	$-\frac{1}{2\sqrt{5}}$	$\frac{3}{5}$
$(\frac{1}{2},\frac{3}{2})$	(1,2)	−2053.464	$\frac{1}{2}$	2	$\frac{3}{2}$	1	4	$\frac{1}{2\sqrt{3}}$	$\frac{1}{3}$
$(\frac{7}{2},\frac{5}{2})$	(3,2)	−1297.079	$\frac{1}{2}$	3	$\frac{7}{2}$	1	24	$-\frac{1}{\sqrt{42}}$	$\frac{12}{21}$
$(\frac{5}{2},\frac{3}{2})$	(3,2)	−1296.096	$\frac{1}{2}$	3	$\frac{5}{2}$	1	12	$\frac{1}{\sqrt{30}}$	$\frac{6}{15}$
$(\frac{5}{2},\frac{5}{2})$	(3,2)	−1255.335	$\frac{1}{2}$	$\frac{5}{2}$	3	2	18	$\frac{1}{3\sqrt{70}}$	$\frac{1}{35}$
$(\frac{3}{2},\frac{1}{2})$	(1,1)	−44.511	$\frac{1}{2}$	1	$\frac{3}{2}$	2	4	$-\frac{1}{6}$	$\frac{1}{9}$
$(\frac{5}{2},\frac{3}{2})$	(2,2)	−41.813	$\frac{1}{2}$	2	$\frac{5}{2}$	2	12	$-\frac{1}{10\sqrt{3}}$	$\frac{1}{25}$
$(\frac{7}{2},\frac{5}{2})$	(3,3)	−41.444	$\frac{1}{2}$	3	$\frac{7}{2}$	2	24	$-\frac{1}{14\sqrt{6}}$	$\frac{1}{49}$
$(\frac{5}{2},\frac{5}{2})$	(2,2)	−1.051	$\frac{1}{2}$	$\frac{5}{2}$	2	4	18	$\frac{\sqrt{7}}{15}$	$\frac{14}{25}$
$(\frac{3}{2},\frac{3}{2})$	(2,2)	−1.051	$\frac{1}{2}$	$\frac{3}{2}$	2	4	8	$-\frac{3}{10\sqrt{2}}$	$\frac{9}{25}$
$(\frac{7}{2},\frac{7}{2})$	(3,3)	+0.309	$\frac{1}{2}$	$\frac{7}{2}$	3	4	32	$\frac{3\sqrt{3}}{28\sqrt{2}}$	$\frac{27}{49}$
$(\frac{5}{2},\frac{5}{2})$	(3,3)	+0.309	$\frac{1}{2}$	$\frac{5}{2}$	3	4	18	$-\frac{\sqrt{10}}{21}$	$\frac{20}{49}$
$(\frac{3}{2},\frac{3}{2})$	(1,1)	+1.054	$\frac{1}{2}$	$\frac{3}{2}$	1	4	8	$\frac{\sqrt{5}}{6\sqrt{2}}$	$\frac{5}{9}$
$(\frac{1}{2},\frac{1}{2})$	(1,1)	+1.054	$\frac{1}{2}$	$\frac{1}{2}$	1	4	2	$-\frac{1}{3}$	$\frac{2}{9}$
$(\frac{3}{2},\frac{5}{2})$	(2,2)	+39.710	$\frac{1}{2}$	2	$\frac{5}{2}$	2	12	$-\frac{1}{10\sqrt{3}}$	$\frac{1}{25}$
$(\frac{5}{2},\frac{7}{2})$	(3,3)	+42.045	$\frac{1}{2}$	3	$\frac{7}{2}$	2	24	$-\frac{1}{14\sqrt{6}}$	$\frac{1}{49}$
$(\frac{1}{2},\frac{3}{2})$	(1,1)	+46.614	$\frac{1}{2}$	1	$\frac{3}{2}$	2	4	$-\frac{1}{6}$	$\frac{1}{9}$
$(\frac{5}{2},\frac{5}{2})$	(2,3)	+1254.584	$\frac{1}{2}$	$\frac{5}{2}$	3	2	18	$\frac{1}{3\sqrt{70}}$	$\frac{1}{35}$
$(\frac{3}{2},\frac{5}{2})$	(2,3)	+1295.345	$\frac{1}{2}$	3	$\frac{5}{2}$	1	12	$\frac{1}{\sqrt{30}}$	$\frac{6}{15}$
$(\frac{5}{2},\frac{7}{2})$	(2,3)	+1296.328	$\frac{1}{2}$	3	$\frac{7}{2}$	1	24	$-\frac{1}{\sqrt{42}}$	$\frac{12}{21}$
$(\frac{3}{2},\frac{1}{2})$	(2,1)	+2053.464	$\frac{1}{2}$	2	$\frac{3}{2}$	1	4	$\frac{1}{2\sqrt{3}}$	$\frac{1}{3}$
$(\frac{5}{2},\frac{3}{2})$	(2,1)	+2058.265	$\frac{1}{2}$	2	$\frac{5}{2}$	1	12	$-\frac{1}{2\sqrt{5}}$	$\frac{3}{5}$
$(\frac{3}{2},\frac{3}{2})$	(2,1)	+2099.027	$\frac{1}{2}$	$\frac{3}{2}$	2	2	8	$\frac{1}{2\sqrt{30}}$	$\frac{1}{15}$

[a] $Z = F$ and $X = F_1$.

[b] Frequency offset in kHz relative to 23722633.335 kHz (Kukolich 1967, Table II)

Table 18. Hyperfine Intensities for NH_3(1,1)

$F' \rightarrow F$	$F_1' \rightarrow F_1$	$J' \rightarrow J$	$\mathrm{R}_i(F_1, J)\mathrm{R}_i(F, F_1)$[a,b]
$(\frac{1}{2}, \frac{1}{2})$	(0,1)	(1,1)	$\frac{1}{27}$
$(\frac{1}{2}, \frac{3}{2})$	(0,1)	(1,1)	$\frac{2}{27}$
$(\frac{3}{2}, \frac{1}{2})$	(2,1)	(1,1)	$\frac{5}{108}$
$(\frac{5}{2}, \frac{3}{2})$	(2,1)	(1,1)	$\frac{1}{12}$
$(\frac{3}{2}, \frac{3}{2})$	(2,1)	(1,1)	$\frac{1}{108}$
$(\frac{1}{2}, \frac{1}{2})$	(1,1)	(1,1)	$\frac{2}{108}$
$(\frac{3}{2}, \frac{1}{2})$	(1,1)	(1,1)	$\frac{1}{108}$
$(\frac{5}{2}, \frac{3}{2})$	(2,2)	(1,1)	$\frac{1}{60}$
$(\frac{3}{2}, \frac{3}{2})$	(2,2)	(1,1)	$\frac{3}{20}$
$(\frac{1}{2}, \frac{3}{2})$	(1,1)	(1,1)	$\frac{1}{108}$
$(\frac{5}{2}, \frac{5}{2})$	(2,2)	(1,1)	$\frac{7}{30}$
$(\frac{3}{2}, \frac{3}{2})$	(1,1)	(1,1)	$\frac{5}{108}$
$(\frac{3}{2}, \frac{5}{2})$	(2,2)	(1,1)	$\frac{1}{60}$
$(\frac{1}{2}, \frac{3}{2})$	(1,2)	(1,1)	$\frac{5}{108}$
$(\frac{3}{2}, \frac{3}{2})$	(1,2)	(1,1)	$\frac{1}{108}$
$(\frac{3}{2}, \frac{5}{2})$	(1,2)	(1,1)	$\frac{1}{12}$
$(\frac{1}{2}, \frac{1}{2})$	(1,0)	(1,1)	$\frac{1}{27}$
$(\frac{3}{2}, \frac{1}{2})$	(1,0)	(1,1)	$\frac{2}{27}$

[a]Compare with Kukolich (1967) Table IX after scaling R_i by $(2I_H + 1)(2I_N + 1) = 6$ (Kukolich (1967) lists unnormalized line strengths in their Table IX).

[b]Note that the sum of the relative intensities $\sum_i R_i = 1.0$.

Table 19. Hyperfine Intensities for $NH_3(2,2)$

$F' \rightarrow F$	$F_1' \rightarrow F_1$	$J' \rightarrow J$	$\mathrm{R}_i(F_1, J)\mathrm{R}_i(F, F_1)$[a,b]
$(\frac{3}{2}, \frac{3}{2})$	(1,2)	(2,2)	$\frac{1}{300}$
$(\frac{3}{2}, \frac{5}{2})$	(1,2)	(2,2)	$\frac{3}{100}$
$(\frac{1}{2}, \frac{3}{2})$	(1,2)	(2,2)	$\frac{1}{60}$
$(\frac{7}{2}, \frac{5}{2})$	(3,2)	(2,2)	$\frac{4}{135}$
$(\frac{5}{2}, \frac{3}{2})$	(3,2)	(2,2)	$\frac{14}{675}$
$(\frac{5}{2}, \frac{5}{2})$	(3,2)	(2,2)	$\frac{1}{675}$
$(\frac{3}{2}, \frac{1}{2})$	(1,1)	(2,2)	$\frac{1}{60}$
$(\frac{5}{2}, \frac{3}{2})$	(2,2)	(2,2)	$\frac{1}{108}$
$(\frac{7}{2}, \frac{5}{2})$	(3,3)	(2,2)	$\frac{8}{945}$
$(\frac{5}{2}, \frac{5}{2})$	(2,2)	(2,2)	$\frac{7}{54}$
$(\frac{3}{2}, \frac{3}{2})$	(2,2)	(2,2)	$\frac{1}{12}$
$(\frac{7}{2}, \frac{7}{2})$	(3,3)	(2,2)	$\frac{8}{35}$
$(\frac{5}{2}, \frac{5}{2})$	(3,3)	(2,2)	$\frac{32}{189}$
$(\frac{3}{2}, \frac{3}{2})$	(1,1)	(2,2)	$\frac{1}{12}$
$(\frac{1}{2}, \frac{1}{2})$	(1,1)	(2,2)	$\frac{1}{30}$
$(\frac{3}{2}, \frac{5}{2})$	(2,2)	(2,2)	$\frac{1}{108}$
$(\frac{5}{2}, \frac{7}{2})$	(3,3)	(2,2)	$\frac{8}{945}$
$(\frac{1}{2}, \frac{3}{2})$	(1,1)	(2,2)	$\frac{1}{60}$
$(\frac{5}{2}, \frac{5}{2})$	(2,3)	(2,2)	$\frac{1}{675}$
$(\frac{3}{2}, \frac{5}{2})$	(2,3)	(2,2)	$\frac{14}{675}$
$(\frac{5}{2}, \frac{7}{2})$	(2,3)	(2,2)	$\frac{4}{135}$
$(\frac{3}{2}, \frac{1}{2})$	(2,1)	(2,2)	$\frac{1}{60}$
$(\frac{5}{2}, \frac{3}{2})$	(2,1)	(2,2)	$\frac{3}{100}$
$(\frac{3}{2}, \frac{3}{2})$	(2,1)	(2,2)	$\frac{1}{300}$

[a]Compare with Kukolich (1967) Table IX after scaling R_i by $(2I_H+1)(2I_N+1) = 6$ (Kukolich (1967) lists unnormalized line strengths in their Table IX).

[b]Note that the sum of the relative intensities $\sum_i R_i = 1.0$.